PRMT1 blockade reverts resistance to KRAS (G12C) inhibition through modulating ferroptosis signalling

XIAOSHUANG FU[1,2*], ZIQI WANG[1,2*], XIAYAO YU[1,2*], HAOLIN SONG[2], HAN SI[1,2], YUCHEN FEI[2], YUHUI LI[2,3], KEYING ZHANG[2,4], YUCE WEI[2], RONGRONG GAO[1,2], RENQING MU[1,2], LING XIE[2,5] and ZHENGBO SONG[1,2]

[1]Postgraduate Training Base Alliance of Wenzhou Medical University (Zhejiang Cancer Hospital), Hangzhou, Zhejiang 310000, P.R. China; [2]Zhejiang Cancer Hospital, Hangzhou Institute of Medicine (HIM), Chinese Academy of Sciences, Hangzhou, Zhejiang 310022, P.R. China; [3]College of Pharmaceutical Science, Zhejiang University of Technology, Hangzhou, Zhejiang 310000, P.R. China; [4]The Second Clinical Medical College, Zhejiang Chinese Medical University, Hangzhou, Zhejiang 310000, P.R. China; [5]Shanghai Immune Therapy Institute, Renji Hospital, Shanghai Jiao Tong University School of Medicine, Shanghai 200127, P.R. China

Received February 17, 2026; Accepted October 19, 2026

DOI: 10.3892/ijo.2026.5958

Abstract. While Kirsten rat sarcoma virus (KRAS) G12C inhibitors (KRAS G12Ci) are successful in clinical practice, their long-term efficacy is limited by acquired resistance, and effective combination strategies are urgently needed. In the present study, pancreatic and lung cancer cell lines resistant to KRAS G12Ci (AMG510/D-1553) were established. Ribonucleic acid-sequencing (RNA-seq) identified significant alterations in ferroptosis-related signaling in KRAS G12Ci-resistant cells. Through *in vivo* and *in vitro* experiments, it was found that an increase occurred in the expression level of protein arginine methyltransferase 1 (PRMT1) in resistant cells. The combined inhibition of KRAS G12C and PRMT1 showed a stronger inhibitory effect on tumor growth than single-target inhibition. Mechanistically, the inhibition of PRMT1 could make histone H4 at arginine 3 (H4R3me2a) less enriched in the promoter region of solute carrier family 7 member 11 (SLC7A11). This suggests that PRMT1 may promote the transcription of SLC7A11 via epigenetic regulation mediated by H4R3me2a. Thus, this inhibits ferroptosis and potentially contributes to the maintenance of the KRAS G12Ci-resistant phenotype. In summary, elevated PRMT1 expression was associated with KRAS G12C inhibitor resistance, and pharmacological inhibition of PRMT1-associated activity enhanced the efficacy of KRAS G12C inhibition partly through ferroptosis. Further genetic validation is required to establish the specific role of PRMT1. The results of the present study will provide new targets and a theoretical basis for overcoming KRAS-targeted treatment resistance, and will also promote the clinical translation of combined therapy.

Correspondence to: Professor Zhengbo Song, Postgraduate Training Base Alliance of Wenzhou Medical University (Zhejiang Cancer Hospital), Hangzhou, Zhejiang 310000, P.R. China
E-mail: songzb@zjcc.org.cn

Dr Ling Xie, Zhejiang Cancer Hospital, Hangzhou Institute of Medicine (HIM), Chinese Academy of Sciences, Hangzhou, Zhejiang 310022, P.R. China
E-mail: xie_xieling@163.com

*Contributed equally

Key words: KRAS G12C, protein arginine methyltransferase 1, ferroptosis, resistance mechanism, combination therapy

Introduction

As one of the most common oncogenes (1), Kirsten rat sarcoma virus (KRAS) belongs to the rat sarcoma virus oncogene family (RAS). The human RAS family is composed of three members, namely KRAS, Harvey rat sarcoma virus (HRAS) and neuroblastoma rat sarcoma virus (NRAS) (2). The RAS protein functions as a guanosine triphosphatase (GTPase) (3). It typically cycles between a bound, inactivated guanosine diphosphate (GDP) state and a bound, activated guanosine triphosphate (GTP) state. This process is under the tight regulation of GTPase-activating proteins (GAPs) and guanine nucleotide exchange factors (GEFs) (4). When KRAS G12C mutates, the 12th amino acid of the KRAS protein changes from glycine to cysteine, which puts KRAS in an active state, bound to GTP (5). The KRAS protein acts as a molecular switch and regulates key signaling pathways. It can be activated by growth factors, chemokines, or receptor tyrosine kinases. Then, activated KRAS activates a variety of downstream signaling pathways, such as the rapidly accelerated fibrosarcoma (RAF)-mitogen-activated protein kinase (MEK)-extracellular signal-regulated kinase (ERK) and phosphoinositide 3-kinase (PI3K)-protein kinase B (AKT)-mammalian target of rapamycin (mTOR) pathways (6-8).

KRAS mutations predominantly involve codon 12. G12D, G12V and G12C represent common mutation subtypes whose prevalence varies across tumor types (9). Despite occurring most frequently in non-small cell lung cancer, KRAS G12C

mutations are also detected in colorectal and pancreatic cancers. Despite its relative uncommonness in pancreatic ductal adenocarcinoma, KRAS G12C is present in ~1-2% of cases. It is a small but clinically relevant molecular subgroup probably benefiting from KRAS G12C-targeted therapy (10). Current efforts primarily target downstream nodes such as MEK, RAF and ERK owing to the difficulties in direct KRAS inhibition (11). However, KRAS-mutated tumors exhibit significant heterogeneity and restrict the efficacy of non-specific targeted therapies against these downstream molecules (12-14). Through binding the switch-II pocket of KRAS G12C in a covalent way, these inhibitors lock the protein in its inactive and GDP-bound state, translating to suppressed downstream signaling (15). Notwithstanding this targeted mechanism, adaptive resistance almost invariably emerges, which paradoxically limits the clinical utility of KRAS G12Ci. Consequently, the formulation of strategies to overcome resistance to KRAS-specific inhibitors is a critical and urgent challenge in the current clinical management of KRAS-mutated tumors.

Characterized by iron accumulation and iron-catalyzed lipid peroxidation, ferroptosis results in oxidative membrane damage and lytic cell death. This distinguishes it from apoptosis, necrosis and autophagy (16,17). Ferroptosis is regulated by cellular metabolism, iron homeostasis, reactive oxygen species (ROS) abundance and other factors. A master regulator of this process is the glutathione (GSH)-glutathione peroxidase 4 (GPX4) axis, reduced by solute carrier family 7 member 11 (SLC7A11). The axis is of great importance in suppressing ferroptosis by neutralizing lipid peroxides (17,18). Given this regulatory mechanism, inducing ferroptosis has become a strategy for overcoming acquired resistance to targeted therapies, which highlights its emerging therapeutic significance (19-21). Targeting this signaling axis can enhance the sensitivity of tumors to ferroptosis to a large extent. Therefore, a core challenge lies in identifying the upstream drivers that abnormally strengthen this signaling axis in drug-resistant cancers. This is because these factors are actionable targets for the re-sensitization of the tumors.

Protein arginine methyltransferase 1 (PRMT1), the primary type I protein arginine methyltransferase, is involved in regulating DNA damage repair, transcription and translation. It plays an important part in the proliferation, metastasis and drug resistance of tumor cells (22). Emerging evidence suggests that PRMT1 regulates ferroptosis in a context-dependent manner. PRMT1 inhibition enhances ferroptosis sensitivity in acute myeloid leukemia through ACSL1 upregulation and has also been reported to reduce radiotherapy resistance in glioma stem cells by promoting ferroptosis (23,24). Conversely, PRMT1 can promote ferroptosis through SLC7A11/FSP1- or EGR1/GLS2-dependent mechanisms in other settings (25,26). Previous research has revealed that PRMT1 renders the SLC7A11 promoter more active (27), which thereby promotes tumor progression by inhibiting ferroptosis. Nevertheless, whether PRMT1 contributes to acquired KRAS G12C inhibitor (KRAS G12Ci) resistance through regulating the SLC7A11-ferroptosis axis has not been established.

In the present study, multiple tumor-derived drug-resistant cell models were successfully established, and no secondary KRAS mutations were demonstrated to occur. This indicates that the drug resistance mainly originated from non-genetic alterations. Transcriptomic analysis identified significant alterations in ferroptosis-related signaling, whereas subsequent functional experiments demonstrated a ferroptosis-resistant phenotype in KRAS G12Ci-resistant cells. Further analysis uncovered elevated PRMT1 expression in established KRAS G12Ci-resistant cells. The present findings are consistent with the involvement of PRMT1-associated H4R3me2a-SLC7A11 signaling in ferroptosis regulation and suggest that ferroptosis contributes to the antitumor effects of the combination treatment. These findings show that the combined inhibition of KRAS G12C and PRMT1 produced greater antitumor activity than either treatment alone in *in vivo* and *in vitro* models. Mechanistically, this combined strategy is capable of disrupting the cellular antioxidant defense system, inducing lipid peroxidation accumulation, and restoring sensitivity to ferroptosis. In this research, elevated PRMT1 expression was observed to be associated with acquired KRAS G12Ci resistance, and the potential involvement of PRMT1 in ferroptosis regulation was investigated. The findings extend the previously described PRMT1-SLC7A11-ferroptosis regulatory framework to the context of KRAS G12Ci resistance. They also confirm that the combined inhibition of KRAS G12C and PRMT1 is a potential therapeutic strategy for resistant tumors.

Materials and methods

Reagents and antibodies. AMG510 and D-1553 were provided by InventisBio. CTS2190 and Ferrostatin-1 were offered by Cytosinlab Therapeutics and MedChemExpress, respectively. Antibodies against GPX4 (cat. no. A25009), glutamate-cysteine ligase modifier subunit (GCLM; cat. no. A5314), PRMT1 (cat. no. A4502), β-Actin (ACTB; cat. no. AC026) and Ki67 (cat. no. A26755PM) were supplied by ABclonal Biotech Co., Ltd. Anti-glyceraldehyde-3-phosphate dehydrogenase (GAPDH; cat. no. ab8245) and anti-SLC7A11 (cat. no. RM5446) antibodies were sourced from Abcam and Biodragon, respectively. Anti-monomethylarginine (MMA; cat. no. 8711) and anti-asymmetric dimethylarginine (ADMA; cat. no. 13522) antibodies were provided by Cell Signaling Technology, Inc. The anti-Histone H4R3me2a antibody was obtained from Active Motif, Inc. Horse radish peroxidase (HRP)-conjugated Goat anti-Rabbit IgG (H+L) (cat. no. AS014) and goat anti-mouse poly-HRP (cat. no. 32230) were bought from ABclonal Biotech Co., Ltd. and Invitrogen; Thermo Fisher Scientific, Inc., respectively.

Cell lines and cell culture. Mia Paca-2 (RRID: CVCL_0428) and H358 (RRID: CVCL_1559) cells were supplied by the Cell Bank of the Chinese Academy of Sciences. Short tandem repeat (STR) profiling was utilized for verifying whether each cell was authentic. Cells were maintained in Dulbecco's Modified Eagle Medium (DMEM) (cat. no. 11965-092; Gibco; Thermo Fisher Scientific, Inc.) or Roswell Park Memorial Institute 1640 (RPMI-1640) medium (cat. no. MA0215; Quickeditbio) supplemented with 10% fetal bovine serum (FBS) (cat. no. FBS500-S; AusGeneX) and 1% penicillin-streptomycin (cat. no. 15140-122; Gibco; Thermo Fisher Scientific, Inc.). Each cell line was cultured at the temperature of 37˚C in

a 5% carbon dioxide (CO_2) environment. The MycoBlue Mycoplasma Detector (cat. no. D101-01; Vazyme Biotech Co., Ltd.) was applied to test all cells for mycoplasma.

Generation and maintenance of KRAS G12Ci-resistant cells. Mia Paca-2 and H358 cells were cultured under conditions with increasing concentrations of AMG510 or D-1553, and subcultured when cells reached 80% confluence. After 4 months of continuous culture of Mia Paca-2 cells, AMG510-resistant Mia Paca-2-510 and H358-510 cell lines at 250 nM, as well as D-1553-resistant Mia Paca-2-1553 and H358-1553 cell lines at 250 nM were selected.

Cell viability assay. Cells were subjected to seeding into a 96-well plate at a density of 3,000-5,000 cells/well and overnight culture. Subsequently, they were treated with dimethyl sulfoxide (DMSO) or the designated drug for a specified duration. DMSO maintained a final concentration of 0.1% in both treatment and control groups. Cell viability was evaluated using the Cell Counting Kit-8 (CCK-8) (cat. no. JR103; Equinox Biotech Co., Ltd.) according to the manufacturer's instructions. Briefly, 10 μl of CCK-8 reagent was added to each well and incubated in the dark at 37˚C in a cell culture incubator for ~30 min, after which the absorbance was measured at 450 nm. The absorbance value of the control group treated with 0.1% DMSO was defined as 100% cell viability. The viability of each treatment group was normalized to this control. CTS2190 concentrations adopted in combination experiments were chosen based on the dose-response profile and half maximal inhibitory concentration (IC_{50}) value of each cell line. Concentrations leading to ~50-70% residual cell viability were employed to avoid excessive single-agent cytotoxicity while allowing assessment of the additional effect of KRAS G12C inhibition.

Colony formation assay. Cells were subjected to seeding at a density of 500 cells/well in a six-well plate and overnight culture. Cultures were maintained under drug-treated and drug-free conditions for specified durations. Following fixation with 4% paraformaldehyde (cat. no. BL539A; Biosharp Life Sciences) and staining with 0.1% crystal violet for 30-min, images were captured. Colonies containing at least 50 cells were manually counted.

ROS level assay. ROS levels were determined using the fluorescent probe 2',7'-Dichlorodihydrofluorescein diacetate (DCFH-DA) as per the ROS Detection Kit (cat. no. S0033S; Beyotime Institute of Biotechnology). DCFH-DA was diluted appropriately in FBS-free medium at a ratio of 1:1,000 to obtain a final concentration of 10 μM. Cells were incubated at the temperature of 37˚C for 30 min, and then washed three times with FBS-free medium. After cell collection, ROS levels were measured using Beckman CytoFlex S and data were analyzed with FlowJo software (v10.8.1; FlowJo LLC).

GSH level assay. GSH content in cells was measured utilizing the GSH Detection Kit (cat. no. S0053; Beyotime Institute of Biotechnology) in accordance with the protocol. Before the measurement of absorbance at 412 nm, GSH concentration in each sample was normalized to protein concentration.

Malondialdehyde (MDA) level assay. The quantification of cellular MDA levels was performed using an MDA Detection Kit (cat. no. S0131S; Beyotime Institute of Biotechnology) according to the instructions of the manufacturer. After normalization to the total protein content of every sample, MDA levels were assessed through the measurement of absorbance at 532 nm.

Mito-Tracker Green staining. Cells were subjected to staining with Mito-Tracker Green (cat. no. C1048; Beyotime Institute of Biotechnology) and Hoechst 33342 (cat. no. C1027; Beyotime Institute of Biotechnology), respectively. Then, they were washed three times with PBS. A confocal laser scanning microscope (Nikon A1RHD25) was leveraged to visualize mitochondria and nuclei in cells.

Chromatin immunoprecipitation-quantitative PCR (ChIP-qPCR). ChIP-qPCR analysis, cells underwent 15-min fixation with 1% formaldehyde, and glycine solution was used to quench the cross-linking reaction. Later, chromatin preparation and immunoprecipitation were performed utilizing the Sonication ChIP Kit (cat. no. RK20258; ABclonal Biotech Co., Ltd.) as per the instructions of the manufacturer. After being purified, the immunoprecipitated DNA was subjected to reverse transcription-quantitative PCR (RT-qPCR) to determine the enrichment of target genomic regions.

RT-qPCR. RNA-easy Isolation Reagent (cat. no. R701-01; Vazyme Biotech Co., Ltd.) was applied to extract total RNA from cell samples. HiScript II Q Select RT SuperMix for qPCR (cat. no. R233-01; Vazyme Biotech Co., Ltd.) was used to synthesize complementary DNA (cDNA) according to the manufacturer's instructions. Then, the synthesized cDNA was subjected to RT-qPCR analysis utilizing a primer mixture and ChamQ Blue Universal SYBR qPCR Master Mix (cat. no. Q312-02; Vazyme Biotech Co., Ltd.). The thermocycling conditions were as follows: Initial denaturation at 95˚C for 30 sec, followed by 40 cycles of denaturation at 95˚C for 10 sec and annealing/extension at 60˚C for 30 sec. Melting curve analysis was performed using the instrument's default program. Primer sequences are shown in Table I. Different genes were normalized relative to ACTB or GAPDH. The ΔΔCq method was employed to compare the relative expression levels of different genes (28).

Western blotting. After cell collection, Radio Immunoprecipitation Assay (RIPA) lysis buffer (cat. no. AIWB-012; Affinibody) was adopted to lyse cells. The bicinchoninic acid Protein Quantification Kit (cat. no. E112-01; Vazyme Biotech Co., Ltd.) was utilized to determine protein concentration. Equal amounts of total protein (10 μg per lane) were mixed with sodium dodecyl sulfate-polyacrylamide gel electrophoresis (SDS-PAGE) loading buffer and separated on 4-20% gradient polyacrylamide gels. After transferring to a polyvinylidene fluoride membrane, cells were blocked with Instant Blocking Buffer (cat. no. AFM-B500; Affinibody) for 15 min at room temperature. The membranes were then incubated overnight at 4˚C with the following primary antibodies at the indicated dilutions: GPX4 (1:4,000), GCLM (1:500), PRMT1 (1:1,000), β-actin (1:200,000), GAPDH (1:5,000), SLC7A11

Table I. Sequences of primers.

Gene name	Primer sequence (5'-3')
GAPDH	F: TCCAAAATCAAGTGGGGCGA
	R: AAATGAGCCCCAGCCTTCTC
β-Actin	F: CTCGCCTTTGCCGATCC
	R: ATCCTTCTGACCCATGCCC
PRMT1	F: CCAGGCGGAAAGCAGTGAGAAG
	R: CCAGCACCACCTTGTCCTTGAAG
GPX4	F: CGCTGTGGAAGTGGATGAAG
	R: TTGTCGATGAGGAACTGTGG
GCLM	F: GAGTTGCACAGCTGGATTCT
	R: CCTCCCAGTAAGGCTGTAAATG
SLC7A11	F: TGTACGAGTCTGGGTGGAAC
	R: TGGTTCCAGAATGTAGCGTCC
LC3B	F: TTCAGGTTCACAAAACCCGC
	R: TCTCACACAGCCCGTTTACC
P21	F: CTCAAATCGTCCAGCGACCT
	R: GACTCCTTGTTCCGCTGCTA
NCOA4	F: GTAGTGATGCACGGAGGGAC
	R: CTGAGCTTTGACCTCTCGCA
KRAS	F: ATTTCGGACTGGGAGCGAGC
	R: CTAACAGTCTGCATGGAGCAGGA
ChIP-q PCR for SLC7A11	F: CAGGACCTACCTACCTGTGG
	R: TGCCAAACAAAAGCAAGCTGA

F, forward; R, reverse; PRMT1, protein arginine methyltransferase 1; GPX4, glutathione peroxidase 4; SLC7A11, solute carrier family 7 member 11; NCOA4, nuclear receptor coactivator 4.

(1:1,000), MMA (1:1,000) and ADMA (1:1,000). Subsequently, the membranes were incubated with the corresponding secondary antibodies (1:2,000) for 1-h at room temperature. The membrane was developed using enhanced chemiluminescence (ECL) Reagent (cat. no. BL520A; Biosharp Life Sciences) chemiluminescence to visualize immunoblotting bands. Densitometric analysis was performed using ImageJ software for the quantitative assessment of protein expression levels. β-Actin was taken as the loading control for most immunoblot analyses. Due to the similar molecular weights (~42 kDa) of PRMT1 and β-Actin, GAPDH was utilized as the loading control for PRMT1 immunoblotting to facilitate reliable band discrimination.

Pathology processing and immunohistochemistry. Collected tumor tissues were subjected to 24-h fixation in 4% paraformaldehyde, dehydration, and then paraffin-embedding. Tissue sections (4-μm thick) were prepared and stained with hematoxylin and eosin (H&E). For immunohistochemical staining, tissue sections were incubated overnight at 4˚C with primary antibodies against GPX4 (1:1,000) or Ki67 (1:1,000), followed by incubation with the corresponding secondary antibodies (1:100) for 1-h at room temperature. Coloring was performed using 3,3'-Diaminobenzidine (DAB) reagents (cat. no. BP055 and BP0771; Biossci; https://www.biossci.com), followed by counterstaining with hematoxylin (cat. no. ZLI-9610; ZSGB-BIO). Tissue sections were scanned using an Olympus VS200 slide scanner (Olympus Corporation), and the images were analyzed using ImageJ2 software (version 2.14.0; National Institutes of Health).

In vivo tumor model. Animal experiments gained the approval of the Hangzhou Institute of Medicine Animal Experiment Ethics Committee (approval no. AP2024-07-0009; Hangzhou, China). Female NOD/ShiLtJGpt-Prkdcem26Cd52Il2rgem26Cd22/Gpt (NCG) mice (n=84; aged 6-8 weeks; weighing 18-20 g) were provided by GemPharmatech Co. Ltd. All mice were kept in a specific-pathogen-free facility maintained at 25˚C and 45-60% relative humidity under a 12/12-h light/dark cycle (lights on at 06:00 and off at 18:00). A total of 6 mice were housed in each cage. They were fed irradiated feed and offered autoclaved tap water. A subcutaneous tumor model was built by injecting $1x10^7$ cells resuspended in 100 μl PBS into the dorsal region of mice on one side. After tumor formation, a Vernier caliper was utilized to measure tumor size every two days until the average tumor volume reached 100 mm^3. In the xenograft models established using parental Mia Paca-2 cells, mice received AMG510 (10 mg/kg), D-1553 (10 mg/kg), CTS2190 (30 mg/kg), or the corresponding combination. In the xenograft models established using KRAS G12Ci-resistant Mia Paca-2-510 or Mia Paca-2-1553 cells, mice received AMG510 (30 mg/kg), D-1553 (30 mg/kg), CTS2190 (30 mg/kg), or a corresponding combination, as appropriate. All drugs were given by oral gavage once a day for 21 consecutive days. AMG510, D-1553, and CTS2190 were formulated in 5% DMSO, 5% Solutol HS-15, and 90% saline. The formula 0.5 x long diameter x short diameter x short diameter was used for the calculation of tumor volume. The maximum tumor volume and diameter recorded during the study were 1,926.68 mm^3 and 16.9 mm, respectively. The tumor size and body weight of NCG mice were measured from the first day of drug administration. All measurements were conducted by investigators who were blinded to group allocation. When the tumor size reached 2,000 mm^3, mice were euthanized by use of CO_2 gas. Mice were euthanized by CO_2 inhalation at a chamber volume displacement rate of 50% per min. Each animal experiment was reported according to the ARRIVE 2.0 guidelines.

Assay of transaminase levels in mouse serum. The Aspartate Aminotransferase Assay Kit (cat. no. C010-2-1; Nanjing Jiancheng Bioengineering Institute) and Alanine Aminotransferase Assay Kit (cat. no. C009-2-1; Nanjing Jiancheng Bioengineering Institute) were used to measure transaminase levels in mouse serum, respectively, following the kit instructions.

RNA-seq and analysis. The RNA of the sample was extracted using TRIzol (cat. no. 15596018; Thermo Fisher Scientific, Inc.). Next, its quality control was carried out utilizing NanoDrop ND-1000 (NanoDrop Technologies; Thermo Fisher Scientific, Inc.) and Bioanalyzer 2100 (Agilent Technologies, Inc.); an A260/280 ratio of 1.8-2.1 and a RIN value >7.0 were deemed acceptable for subsequent experiments. Oligo (dT) magnetic beads [Dynabeads Oligo (dT); cat. no. 25-61005; Thermo Fisher Scientific, Inc.] were

utilized for specifically capturing the mRNA containing PolyA(polyadenylic acid). The sequencing (seq) of RNA libraries was performed by LC Bio Technology Co., Ltd. on the Illumina NovaseqTM 6000 platform (Illumina, Inc.) with a paired-end (PE150) configuration, yielding a read length of 150 bp. The final libraries were quantified using qPCR, and the loading concentration for sequencing was 190 pM. For data analysis, raw reads were verified using FastQC (v0.11.9). Clean reads were aligned to the human reference genome using HISAT2 (v2.2.1). The mapped reads were assembled using StringTie (v2.1.6) and merged using gffcompare (v0.9.8). Differentially expressed genes were identified using DESeq2 (for group comparisons) and edgeR (for two-sample comparisons).

Sanger sequencing. After being extracted from cell samples, total RNA was converted into cDNA. Primers, cDNA and 2X Taq Master Mix (cat. no. P111-03; Vazyme Biotech Co., Ltd.) were mixed and amplified by PCR as per the instructions of the manufacturer. PCR products were subjected to Sanger seq site validation, which was outsourced to Sangon Biotech Co., Ltd.

Statistical analysis. For all experiments, n denotes independent biological replicates. When performed, technical replicates were not regarded as independent observations for statistical analysis. For *in vivo* experiments, each mouse was viewed as one biological replicate. However, independent tumor tissues obtained from different mice were deemed as biological replicates for *ex vivo* analyses. Data were expressed as the mean ± standard error of mean (SEM). GraphPad Prism 9.0 software (Dotmatics) was applied to perform statistical analyses. $P<0.05$ was considered to indicate statistically significant differences. Statistical analyses employed unpaired two-tailed Student's t-tests, one-way analysis of variance (ANOVA), or two-way ANOVA followed by Tukey's multiple comparison tests, as appropriate.

Results

Constructed cell lines resistant to KRAS G12Ci. To investigate the mechanisms of resistance to KRAS G12Ci, resistant cell lines derived from parental Mia Paca-2 and H358 cells were cultured. Through continuous exposure to increasing concentrations of KRAS G12Ci (AMG510 or D-1553) over 4 months, resistant cell lines were established. They included Mia Paca-2-510 and H358-510 cell lines (resistant to 250 nM AMG510), and Mia Paca-2-1553 and H358-1553 cell lines (resistant to 250 nM D-1553). To validate resistance, the IC_{50} values of sensitive Mia Paca-2 cells (Fig. 1A), resistant Mia Paca-2-510 cells (Fig. 1B) and Mia Paca-2-1553 cells (Fig. 1C) after five-day exposure to KRAS G12Ci AMG510 and D-1553 were measured, respectively. In addition, the IC_{50} value of the PRMT1 inhibitor (PRMT1i) CTS2190 was also determined. The IC_{50} value of the resistant strain Mia Paca-2-510 was 130.65 μM, while that of Mia Paca-2-1553 was 16.47 μM. These IC_{50} values represented 3,510-fold and 1,340-fold increases, respectively, which successfully identified KRAS G12Ci-resistant cells. The same method was adopted to determine the IC_{50} values of sensitive and drug-resistant H358 against three drugs (Fig. 1D-F). Prior studies have revealed that acquired resistance to KRAS G12Ci can involve secondary KRAS alterations at various residues, including mutations influencing the switch-II pocket and other KRAS regulatory sites (1). Sanger sequencing was performed to determine the presence of secondary KRAS alterations in Mia Paca-2-derived resistant models. No additional KRAS mutations were observed in the sequenced region of Mia Paca-2-510 and Mia Paca-2-1553 cells (Fig. 1G), with the original KRAS G12C mutation retained. This suggests that resistance in these models may involve non-mutational mechanisms.

Transcriptomic analysis identifies ferroptosis-related alterations in KRAS G12C inhibitor-resistant cells. To investigate the molecular alterations associated with acquired resistance to KRAS G12C inhibition, RNA-seq analysis was conducted to compare drug-resistant Mia Paca-2-510 and Mia Paca-2-1553 strains with parental Mia Paca-2, followed by Kyoto Encyclopedia of Genes and Genomes (KEGG) enrichment analysis. KEGG pathway enrichment analysis of differentially expressed genes identified ferroptosis among the significantly enriched pathways in both resistant cell models (Fig. 2A and B). To provide a comprehensive overview of the transcriptional differences between parental and resistant cells, volcano plots were generated using a threshold of $|\log2 \text{ fold change}|>1$ and $P<0.05$. These analyses revealed widespread transcriptional alterations in both Mia Paca-2-510 and Mia Paca-2-1553 cells compared with parental Mia Paca-2 cells (Fig. 2C and D). Notably, the transcriptomic changes in ferroptosis-related genes did not exhibit a uniformly directional pattern consistent with simple activation or suppression of ferroptosis. Therefore, the RNA-seq data were interpreted as indicating perturbation of ferroptosis-related signaling rather than directly defining the functional state of ferroptosis. These transcriptomic findings provided the rationale for further examination of ferroptosis-associated molecular and biochemical features in resistant cells. RT-qPCR confirmed the upregulated mRNA expression of genes inhibiting ferroptosis [*GPX4*, *SLC7A11* and cyclin-dependent kinase inhibitor 1A *(CDKN1A)*] and the downregulated expression of genes promoting ferroptosis [nuclear receptor coactivator 4 (*NCOA4)*] and microtubule-associated protein 1 light chain 3 beta (*MAP1LC3B*) in resistant strains (Fig. 3A). Western blot analysis further revealed the increased protein expression of GPX4 and GCLM, two ferroptosis-suppressing proteins, in the resistant strain (Figs. 3B and S1A). Moreover, the measurement of ROS levels using the fluorescent probe DCFH-DA indicated significantly reduced ROS in resistant strains compared with the sensitive strain (Fig. 3C and D). The aforementioned results suggested that the levels of ferroptosis-related markers and the expression of relevant regulatory molecules were changed in drug-resistant cells. This indicates that ferroptosis resistance may play a vital role in developing KRAS G12Ci resistance.

Targeting PRMT1 can restore the sensitivity of drug-resistant cells to KRAS G12Ci in vitro. KRAS G12Ci-resistant cells were demonstrated to exhibit a pronounced ferroptosis resistance phenotype. It has been reported that PRMT1 plays a regulatory role as a transcriptional activator of SLC7A11. In addition, the increase in the expression level

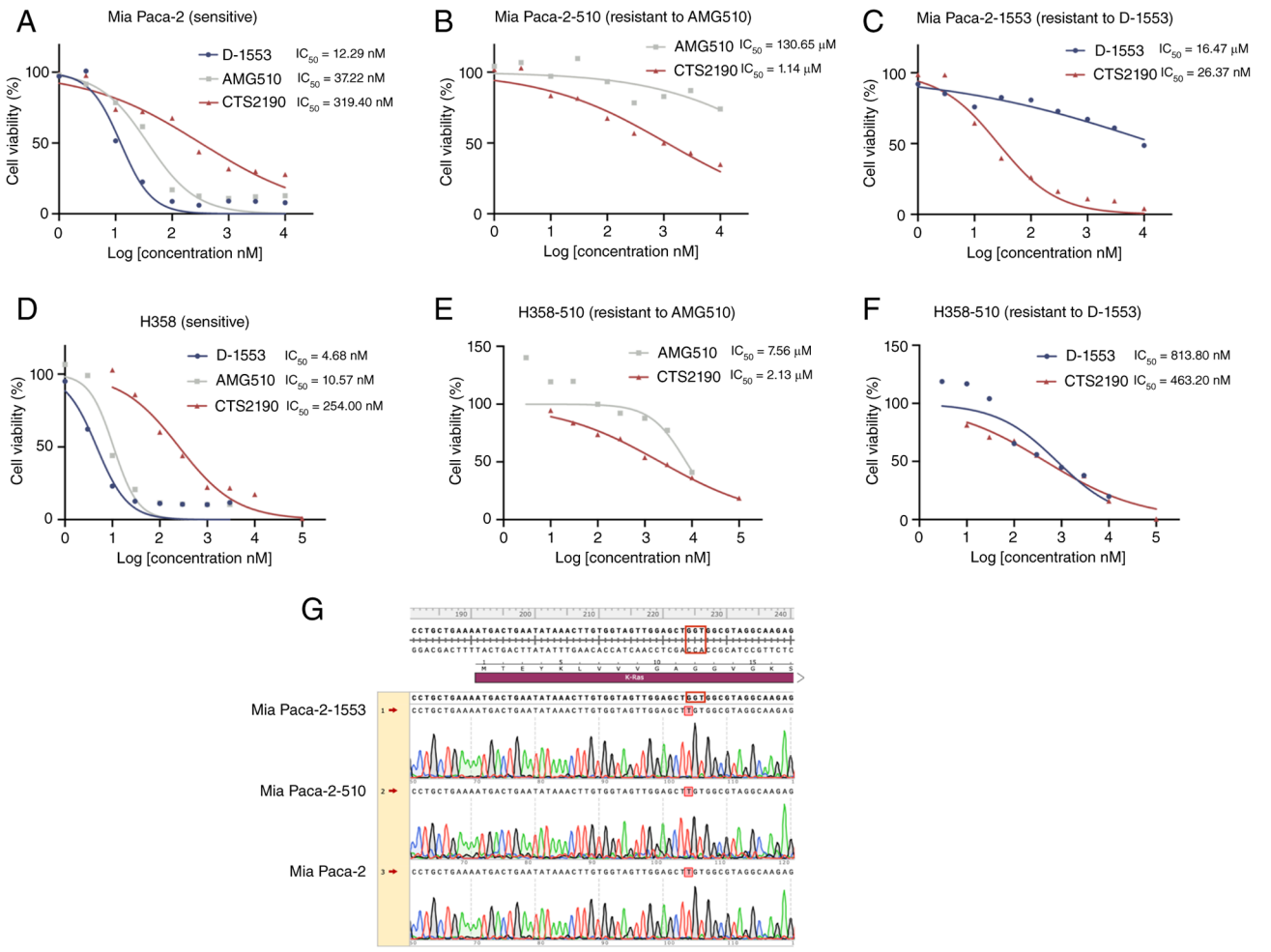


Figure 1. Establishment and characterization of KRAS G12C inhibitor-resistant cell lines. (A) Cell viability of Mia Paca-2 cells after 5 days of treatment with increasing concentrations of AMG510, D-1553, or CTS2190 (n=4). (B and C) Cell viability of the corresponding resistant cell lines, Mia Paca-2-510 and Mia Paca-2-1553, after 5 days of treatment with increasing concentrations of the indicated inhibitors (n=4). (D) Cell viability of parental H358 cells after 5 days of treatment with increasing concentrations of AMG510, D-1553, or CTS2190 (n=4). (E and F) Cell viability of the corresponding resistant cell lines, H358-510 and H358-1553, after 5 days of treatment with increasing concentrations of the indicated inhibitors (n=4). (G) Sanger sequencing analysis of the KRAS sequence in parental Mia Paca-2, Mia Paca-2-510 and Mia Paca-2-1553 cells. Data are presented as the mean ± SEM. One-way ANOVA for multi-group comparisons.

of SLC7A11 can enhance the ability of tumor cells to clear lipid peroxides, which thereby provides their resistance to ferroptosis (27). On this basis, whether PRMT1 regulates the transcription of SLC7A11 through an epigenetic mechanism was further explored. The ChIP-qPCR results revealed a significant reduction in the enrichment level of H4R3me2a in the promoter region of SLC7A11 after PRMT1 inhibition (Fig. 4A). This suggests that PRMT1 possibly participates in the transcriptional activation of SLC7A11 via the promotion of H4R3me2a modification in this region. Therefore, it was hypothesized that the ferroptosis-resistant phenotype noted in KRAS G12Ci-resistant cells might be linked to elevated PRMT1 expression. To further investigate this possibility, the expression of PRMT1 in resistant and parental cells was examined. RT-qPCR and western blotting uncovered a significant increase in *PRMT1* mRNA and PRMT1 protein expression in resistant cells compared with parental cells (Fig. 4B and C; Fig. S1B). This indicates that elevated PRMT1 expression is related to the established KRAS G12Ci-resistant phenotype. These findings prompted researchers to further evaluate PRMT1 as an underlying therapeutic target in resistant cells. Global arginine methylation levels were examined by western blotting for the purpose of confirming the pharmacological activity of the PRMT1 inhibitor CTS2190 in pancreatic cancer cells. CTS2190 treatment resulted in a remarkable reduction in ADMA, accompanied by an increase in MMA levels (Fig. 4D and E). This is consistent with the inhibition of arginine methylation mediated by type I PRMT. These findings confirmed the expected pharmacodynamic activity of CTS2190 in the experimental system of the present study.

Based on these findings, the present study aimed to determine whether a combination strategy could reverse KRAS G12C resistance. To validate the efficacy of combination therapy, tumor cells were treated with two KRAS G12Ci (AMG510/D-1553) *in vitro*, each of which was combined with PRMT1i (CTS2190). The colony formation experiment clearly demonstrated that the proliferation of pancreatic cancer cells in the combined group was greatly inhibited (Fig. 4F). Cell viability measured by CCK-8 assay verified that combination

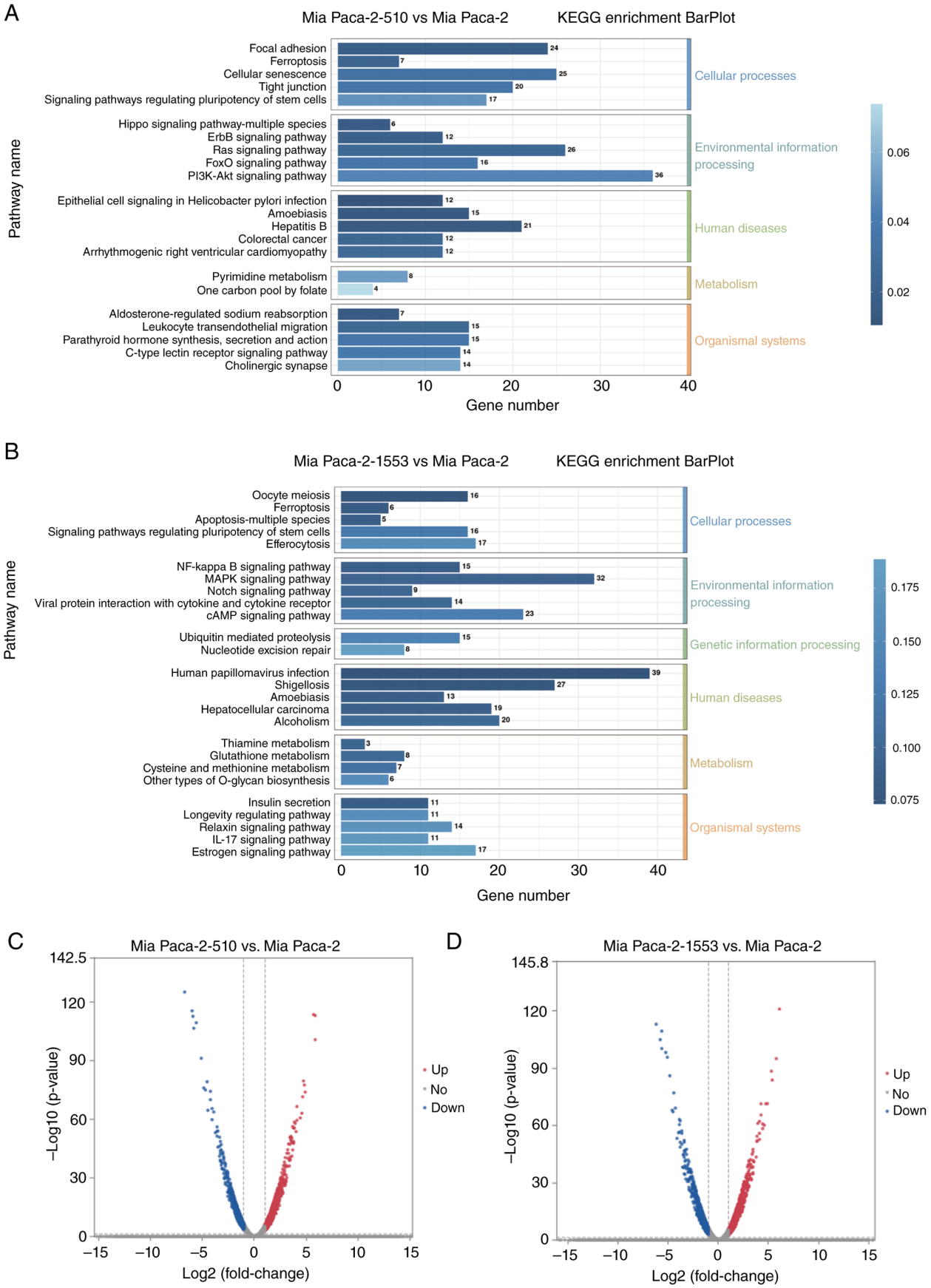


Figure 2. Transcriptomic alterations associated with acquired KRAS G12C inhibitor resistance. (A) KEGG pathway enrichment analysis of DEGs between Mia Paca-2-510 and Mia Paca-2 cells based on RNA-seq. (B) KEGG pathway enrichment analysis of DEGs between Mia Paca-2-1553 and Mia Paca-2 cells based on RNA-seq. (C) Volcano plot showing the global distribution of DEGs between Mia Paca-2-510 and Mia Paca-2 cells. (D) Volcano plot showing the global distribution of DEGs between Mia Paca-2-1553 and Mia Paca-2 cells. Genes with |log2 fold change|>1 and P<0.05 were defined as significantly differentially expressed. Upregulated and downregulated genes are indicated separately, whereas genes not meeting these criteria are shown as non-significant. KEGG, Kyoto Encyclopedia of Genes and Genomes; DEGs, differentially expressed genes; RNA-seq, RNA sequencing.

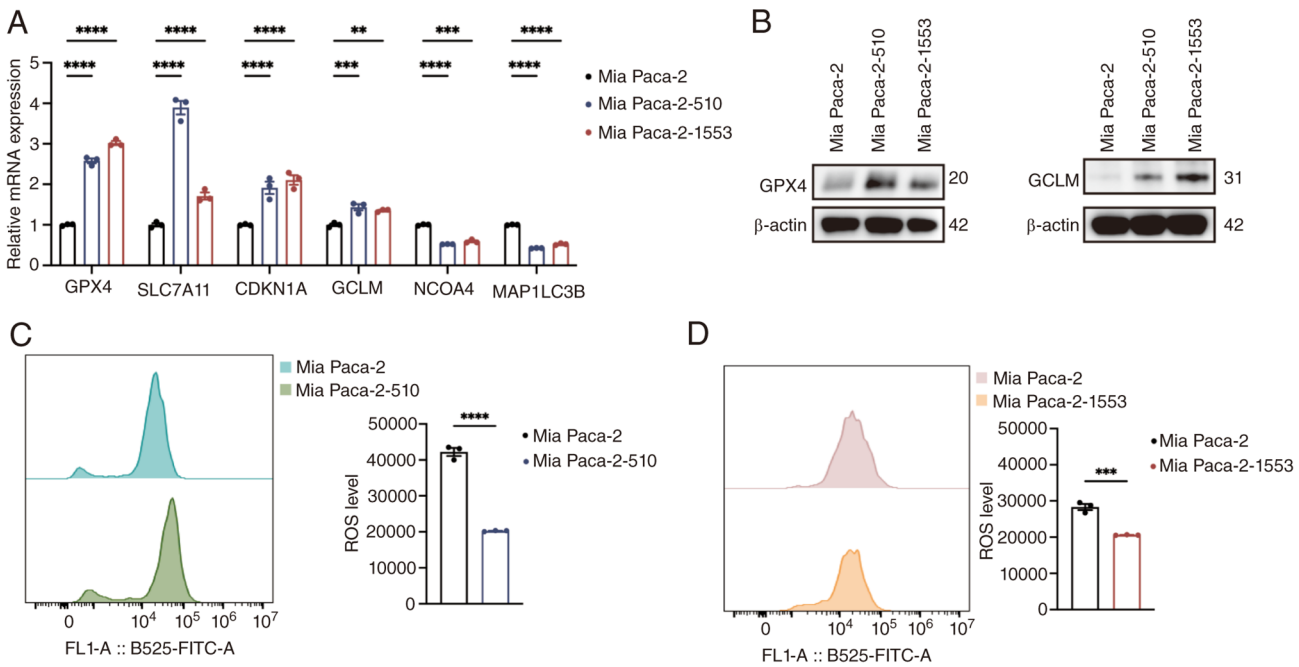


Figure 3. KRAS G12C inhibitor-resistant cells exhibit a ferroptosis-resistant phenotype. (A) Reverse transcription-quantitative PCR analysis of ferroptosis-related genes in parental and KRAS G12C inhibitor-resistant cells (n=3). (B) Western blot analysis of GPX4 and GCLM protein expression in parental and resistant cells. (C) Intracellular ROS levels in Mia Paca-2 and Mia Paca-2-510 cells measured using the fluorescent probe DCFH-DA (n=3). (D) Intracellular ROS levels in Mia Paca-2 and Mia Paca-2-1553 cells measured using the fluorescent probe DCFH-DA (n=3). Data are presented as the mean ± SEM. Statistical significance was determined by one-way ANOVA for multiple-group comparisons and unpaired two-tailed Student's t-test for two-group comparisons. **P<0.01, ***P<0.001 and ****P<0.0001. GPX4, glutathione peroxidase 4; ROS, reactive oxygen species; SLC7A11, solute carrier family 7 member 11; NCOA4, nuclear receptor coactivator 4; MAP1LC3B, microtubule-associated protein 1 light chain 3 beta.

therapy suppressed the proliferation of Mia Paca-2 cells more effectively than either agent alone (Fig. 4G and H). In two drug-resistant cell lines, it was subsequently confirmed that the combination therapy group showed markedly slowed tumor cell proliferation compared with the monotherapy one (Fig. 4I and J). The Chou-Talalay method was adopted to further assess drug combination effects in Mia Paca-2, Mia Paca-2-510 and Mia Paca-2-1553 cells. The purpose was to quantitatively evaluate the interaction between KRAS G12C and PRMT1 inhibition. Combination index (CI) analysis revealed that the two drugs synergistically interacted with each other at lower effect levels, as indicated by CI values below 1 (Fig. S2A-D). To further assess the generalizability of this combination strategy, experiments were extended to H358, a KRAS G12C-mutant lung cancer cell line, and its resistant derivatives. The results revealed a comparable enhancement of growth inhibition by the combination treatment (Fig. S3A-H). Overall, these results suggest that combining KRAS G12Ci with PRMT1i can potently inhibit the proliferation of KRAS G12C tumor cells *in vitro*.

Combination of KRAS G12Ci and PRMT1i inhibits tumor growth in vivo. A subcutaneous tumor model was established using NCG mice, with the aim of further validating the inhibitory effect of combination therapy on the proliferation of KRAS G12C cells *in vivo*. Each of Mia Paca-2, Mia Paca-2-510 and Mia Paca-2-1553 cells was injected subcutaneously into the dorsal region of every female NCG mouse. When the average tumor volume reached 100 mm^3, mice received daily oral doses of either solvent, KRAS G12Ci, PRMT1i or both drugs combined, in light of the dosing regimen illustrated in Fig. 5A. In the Mia Paca-2 subcutaneous tumor model, the combination therapy group exhibited significantly smaller tumor volumes (Fig. 5B-D; Fig. S4A) and decreased expression of the proliferation marker Ki67 compared with both control and single-agent groups (Fig. 5E and F). H&E staining revealed extensive tumor necrosis and marked tissue destruction in the combination treatment group (Fig. S4B), which indicated enhanced antitumor efficacy. This suggests that the combination of KRAS G12Ci and PRMT1i promotes tumor regression *in vivo*. As presented in Figs. 6A-F and S4C and D, in the model established with drug-resistant cells, the combination group exhibited significantly lower tumor volume and Ki67 expression compared with the control group. H&E staining showed increased tumor necrosis after combination treatment, which indicated enhanced tumor cell damage (Fig. S4E). These results show that the combination treatment retains significant antitumor activity in KRAS G12Ci-resistant xenograft models, although the magnitude of the response was more modest than that observed in the parental model. As demonstrated in Fig. S5A, serum transaminase levels in mice across all treatment groups were not significantly different, which indicated no apparent hepatotoxicity from drug treatment. H&E staining revealed that tumor metastasis was markedly reduced in the KRAS G12Ci + PRMT1i group despite the clear visibility of tumor metastasis in the liver tissue of the control group (Fig. S5B). Collectively, these results demonstrate that combined KRAS G12Ci and PRMT1i therapy can delay KRAS G12C tumor progression *in vivo*.

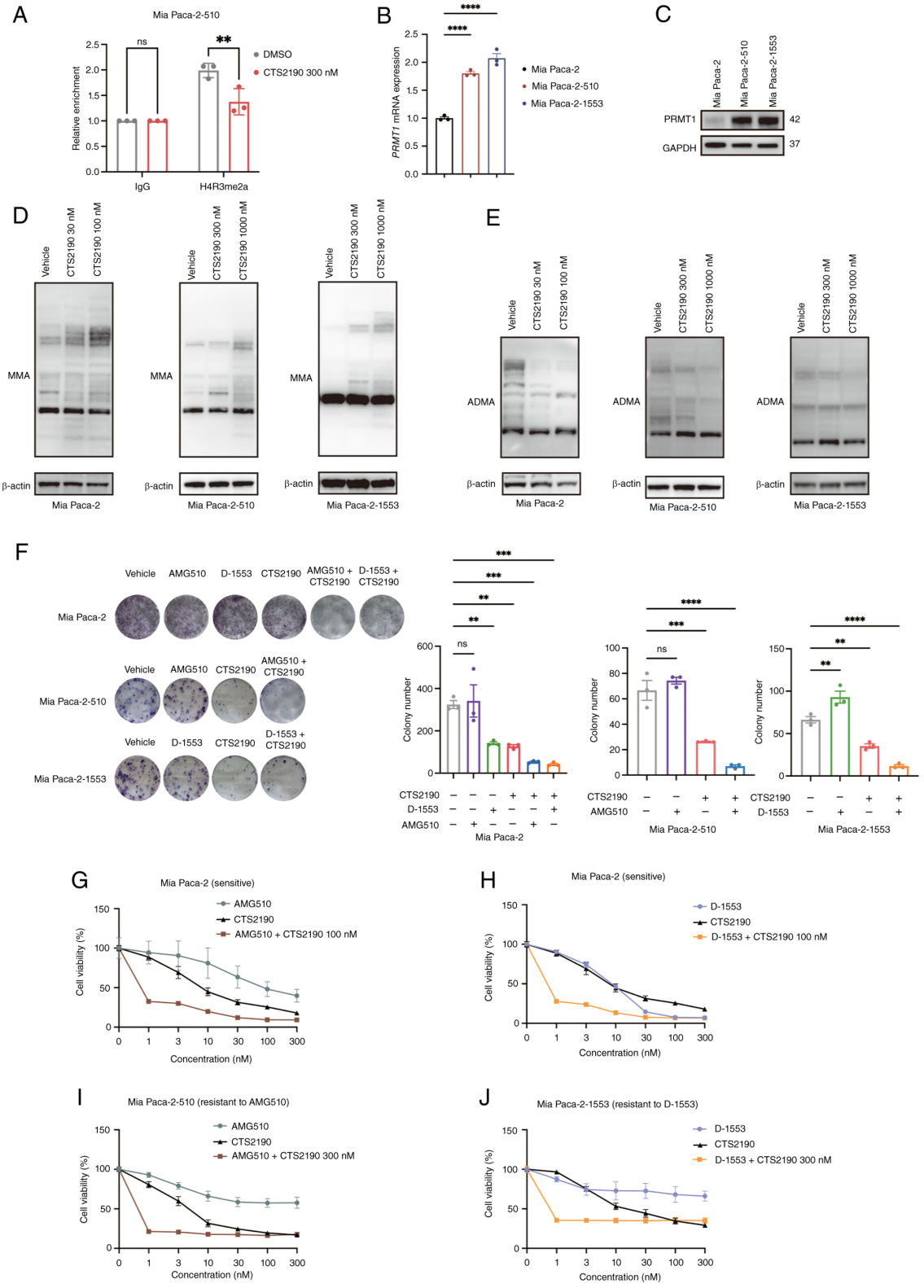


Figure 4. Targeting PRMT1 can reverse drug resistance in KRAS G12C mutant cells *in vitro*. (A) Chromatin immunoprecipitation-quantitative PCR analysis of H4R3me2a enrichment at the SLC7A11 promoter in Mia Paca-2-510 cells following CTS2190 treatment. IgG was used as a negative control (n=3). (B) Reverse transcription-quantitative PCR analysis of *PRMT1* mRNA expression in Mia Paca-2, Mia Paca-2-510 and Mia Paca-2-1553 cells (n=3). (C) Western blot analysis of PRMT1 protein expression in Mia Paca-2, Mia Paca-2-510 and Mia Paca-2-1553 cells (n=3). (D and E) Western blot analysis of MMA and ADMA levels in Mia Paca-2, Mia Paca-2-510 and Mia Paca-2-1553 cells following treatment with CTS2190 at the indicated concentrations (n=3). (F) Colony formation assays evaluating the effects of KRAS G12C inhibitors (AMG510 or D-1553), CTS2190, or their combinations in Mia Paca-2 and the corresponding resistant cells. Representative images and colony quantification are shown (n=3). (G and H) CCK-8 assays evaluating the effects of AMG510 or D-1553 combined with CTS2190 on Mia Paca-2 cells after 5 days of treatment (n=4). (I) CCK-8 assay evaluating the effect of AMG510 combined with CTS2190 on Mia Paca-2-510 cells after 5 days of treatment (n=4). (J) CCK-8 assay evaluating the effect of D-1553 combined with CTS2190 on Mia Paca-2-1553 cells after 5 days of treatment (n=4). Data are presented as the mean ± SEM. One-way ANOVA for multi-group comparisons. **P<0.01, ***P<0.001 and ****P<0.0001. PRMT1, protein arginine methyltransferase 1; MMA, global monomethylarginine; ADMA, asymmetric dimethylarginine; CCK-8, Cell Counting Kit-8; ns, not statistically significant.

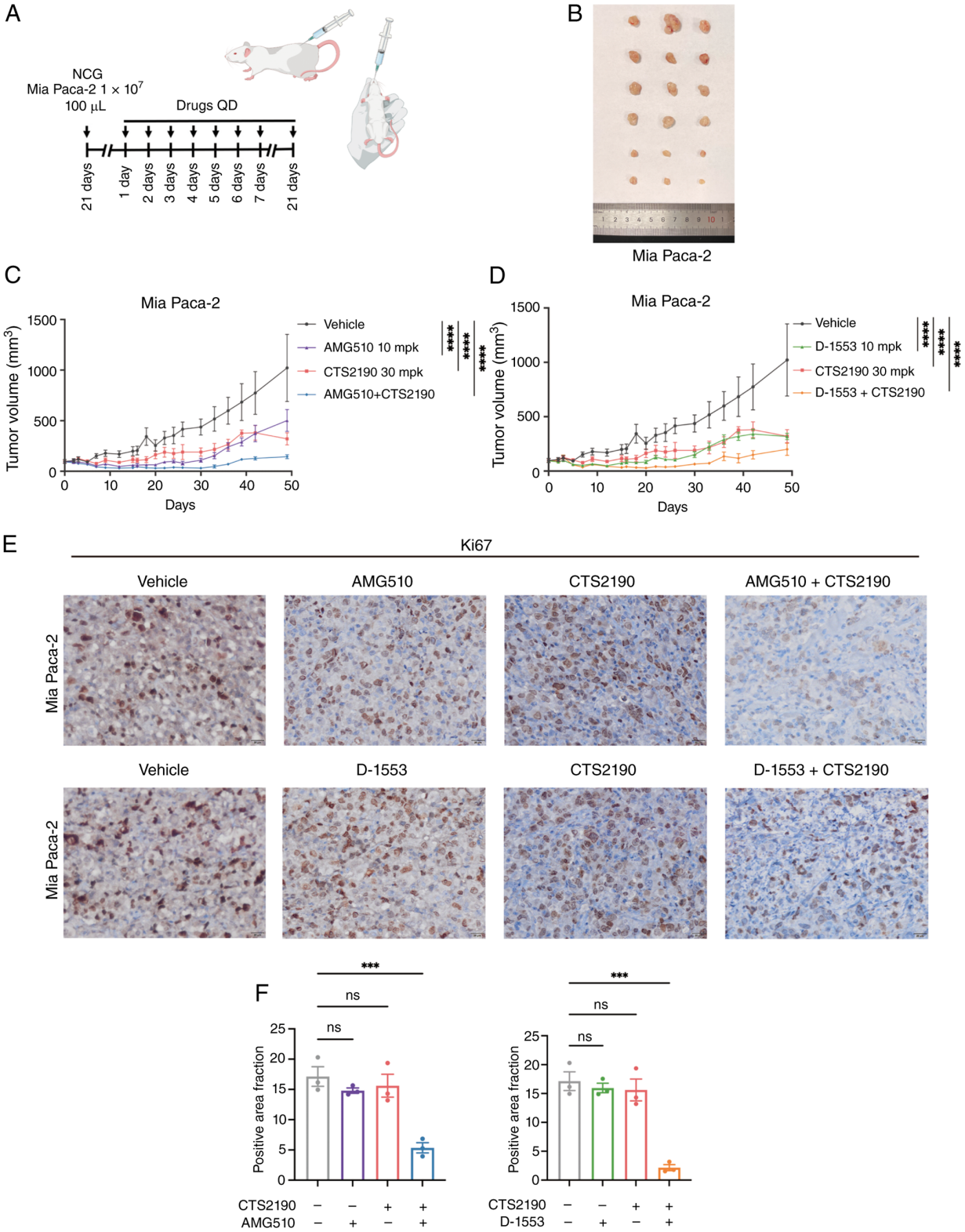


Figure 5. KRAS G12Ci combined with protein arginine methyltransferase 1 inhibitor inhibit tumor growth in mouse models. (A) Schematic of drug administration after subcutaneous tumor implantation in NCG mice, created with BioGDP.com (43). (B) Representative images of excised Mia Paca-2 xenograft tumors from the different treatment groups. (C and D) Tumor growth curves of Mia Paca-2 xenografts treated with AMG510 or D-1553 alone or in combination with CTS2190 (n=6). Two-way ANOVA for multi-group comparisons. (E) Representative immunohistochemical staining of Ki67 in Mia Paca-2 xenograft tumors from the indicated treatment groups. Scale bars, 20 μm. (F) Quantification of Ki67-positive area fractions in tumor tissues (n=3). Data are presented as the mean ± SEM. One-way ANOVA for multi-group comparisons. ***P<0.001 and ****P<0.0001. ns, not statistically significant.

Targeting PRMT1 promotes ferroptosis in KRAS G12C-resistant cells. The present study sought to validate whether combined treatment with KRAS G12Ci and PRMT1i could induce ferroptosis in tumor cells for further investigation. After combined treatment, Mito-Tracker Green staining was used to evaluate mitochondrial morphology. Mia Paca-2 cells

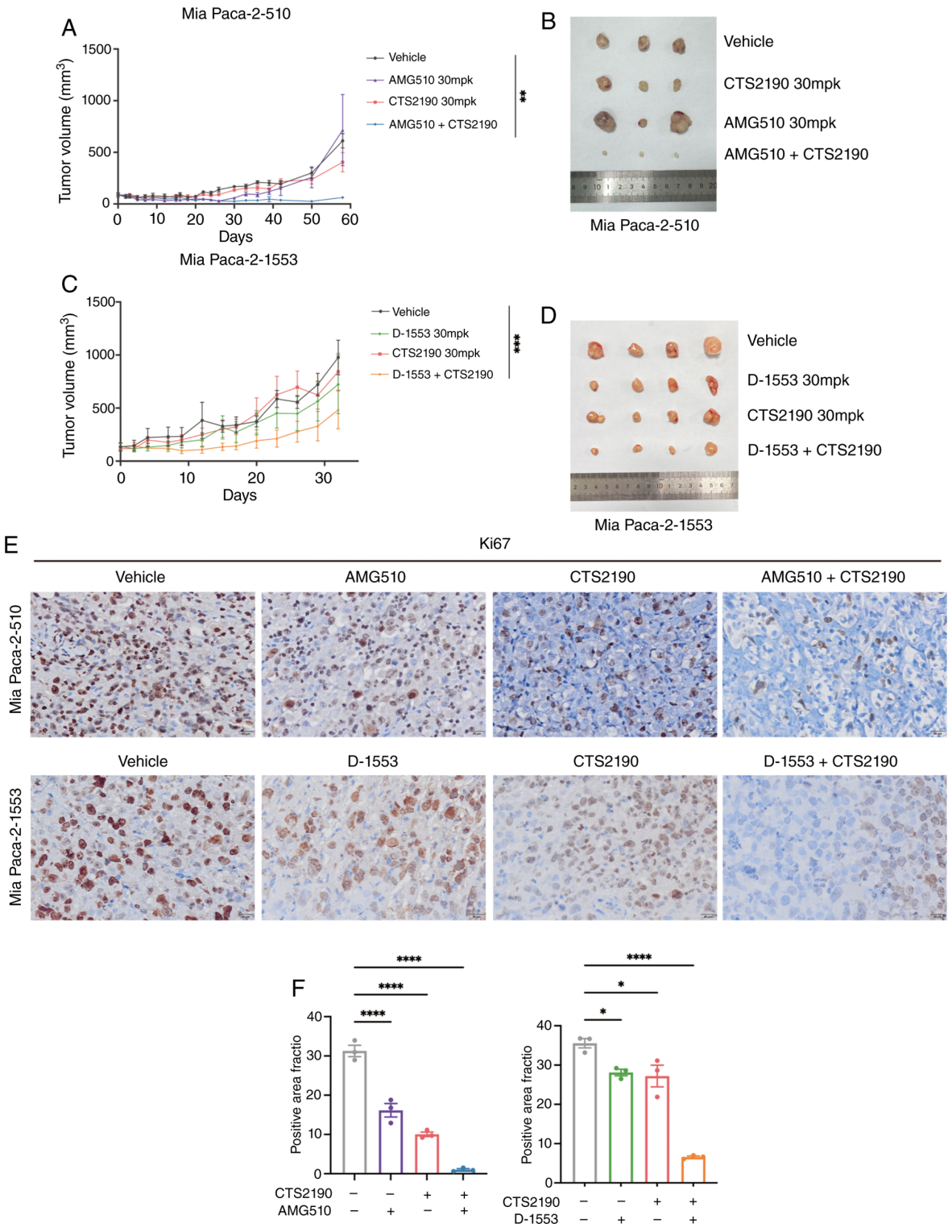


Figure 6. KRAS G12Ci suppresses tumor growth in drug-resistant mouse models in conjunction with protein arginine methyltransferase 1 inhibitor. (A) Tumor growth curves of Mia Paca-2-510 xenografts treated with vehicle, AMG510, CTS2190, or AMG510 plus CTS2190 (n=6). Two-way ANOVA for multi-group comparisons. (B) Representative images of excised Mia Paca-2-510 xenograft tumors from the indicated treatment groups. (C) Tumor growth curves of Mia Paca-2-1553 xenografts treated with vehicle, D-1553, CTS2190, or D-1553 plus CTS2190 (n=6). Two-way ANOVA for multi-group comparisons. (D) Representative images of excised Mia Paca-2-1553 xenograft tumors from the indicated treatment groups. (E) Representative immunohistochemical staining of Ki67 in Mia Paca-2-510 and Mia Paca-2-1553 xenograft tumors after the indicated treatments. Scale bars, 20 μm. (F) Quantification of Ki67-positive area fractions in the corresponding tumor tissues (n=3). Data are presented as the mean ± SEM. One-way ANOVA for multi-group comparisons. *P<0.05, **P<0.01, ***P<0.001 and ****P<0.0001.

exhibited apparent alterations in mitochondrial morphology in comparison to the other treatment groups (Fig. 7A). Total GSH levels demonstrated a significant decrease in drug-resistant cells after combination treatment compared with either monotherapy, which indicated the depletion of the intracellular glutathione pool (Fig. 7B). Furthermore,

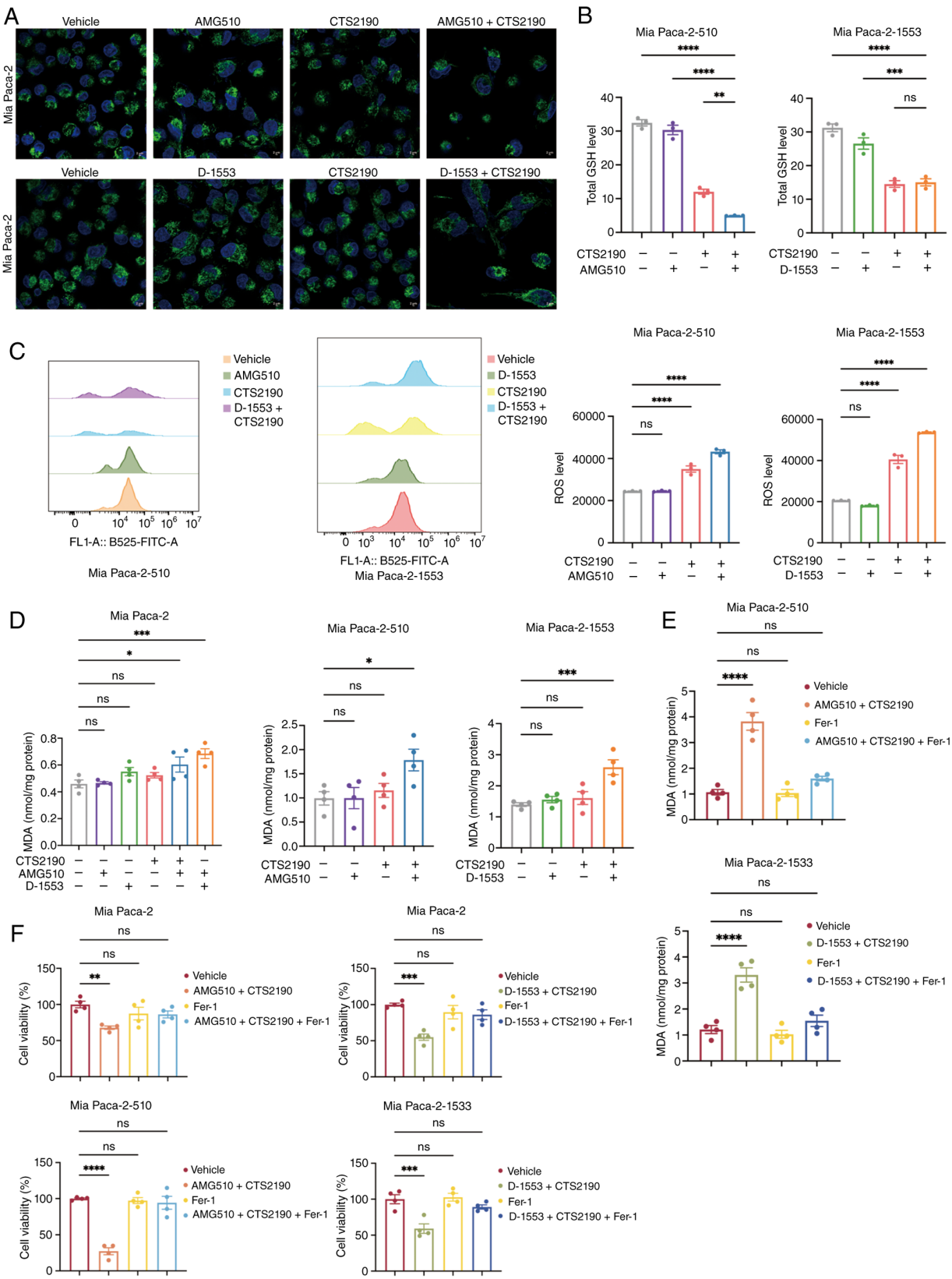


Figure 7. Combined inhibition of KRAS G12C and protein arginine methyltransferase 1 promotes ferroptosis in parental and KRAS G12C inhibitor-resistant cells. (A) Representative confocal images of mitochondrial morphology in Mia Paca-2 cells following treatment with vehicle, KRAS G12C inhibitor, CTS2190, or the indicated combination. Mitochondria were stained with Mito-Tracker Green and nuclei with Hoechst 33342. Scale bars, 2 μm. (B) Total GSH levels in Mia Paca-2-510 and Mia Paca-2-1553 cells following the indicated treatments (n=3). (C) Representative flow cytometry profiles and quantification of intracellular ROS levels in Mia Paca-2-510 and Mia Paca-2-1553 cells following the indicated treatments (n=3). (D) MDA levels in Mia Paca-2, Mia Paca-2-510 and Mia Paca-2-1553 cells following treatment with KRAS G12C inhibitor, CTS2190, or their combination (n=4). (E) MDA levels in Mia Paca-2-510 and Mia Paca-2-1553 cells after combination treatment in the presence or absence of the ferroptosis inhibitor Ferrostatin-1 (Fer-1) (n=4). (F) Cell Counting Kit-8 assays assessing cell viability in Mia Paca-2, Mia Paca-2-510, and Mia Paca-2-1553 cells following combination treatment with or without Fer-1 (n=4). Data are presented as the mean ± SEM. One-way ANOVA for multi-group comparisons. *P<0.05, **P<0.01, ***P<0.001 and ****P<0.0001. ROS, reactive oxygen species; MDA, malondialdehyde; ns, not statistically significant.

the flow cytometric analysis of ROS levels in drug-resistant tumor cells revealed that the combination therapy group revealed a significant increase in ROS levels (Fig. 7C). This is in line with the increased accumulation of ROS. MDA levels exhibited a significant elevation after combination treatment compared with either monotherapy in Mia Paca-2 cells and corresponding drug-resistant cells (Fig. 7D), which further indicated enhanced lipid peroxidation. The ferroptosis inhibitor markedly attenuated the combination-induced increase in MDA levels in drug-resistant cells, and MDA levels were not significantly different from those in the control group (Fig. 7E). This further supported the involvement of ferroptosis-associated lipid peroxidation. Finally, rescue experiments demonstrated that the ferroptosis inhibitor markedly restored cell viability in Mia Paca-2 cells and corresponding drug-resistant cells exposed to the combination treatment (Fig. 7F). Thus, the involvement of ferroptosis in combination-induced cell death was further confirmed.

To further clarify the mechanism, RT-qPCR and western blotting were utilized for detecting changes in ferroptosis-associated genes and proteins after combined treatment with KRAS G12Ci and PRMT1i. The results indicated a significant downregulation in the mRNA levels of *GPX4*, *SLC7A11*, and *GCLM*, as well as the corresponding protein levels in both sensitive and resistant cells (Fig. 8A-D; Fig. S6A and B). These findings demonstrate that combined KRAS G12Ci and PRMT1i therapy suppresses the proliferation of KRAS G12C cells by promoting ferroptosis signaling pathways.

Next, the immunohistochemical analysis of tumor tissues gathered from animal experiments revealed the reduced expression of GPX4 after combined KRAS G12Ci and PRMT1i treatment (Fig. 9A and B). Similarly, *in vivo* experiments demonstrated that the combined inhibition of KRAS G12C and PRMT1 inhibits tumor growth by activating ferroptosis.

A schematic diagram was included to more clearly elucidate the mechanism by which targeting PRMT1 inhibits tumor progression through regulating of ferroptosis pathway (Fig. 10).

Discussion

KRAS G12C inhibition resistance has frequently been attributed to secondary genetic alterations or the reactivation of oncogenic signaling (29). However, the findings of the present study suggest that epigenetic and redox adaptation may also contribute to the resistant state. In the present study, ferroptosis resistance was identified as a potential adaptive phenotype associated with acquired KRAS G12Ci resistance, and PRMT1 was further determined as a potential upstream regulator of this process. The pharmacological inhibition of PRMT1 enhanced the antitumor activity of KRAS G12Ci in both resistant and parental tumor models. This suggests that the PRMT1-ferroptosis axis represents a possible therapeutic vulnerability in KRAS G12C-mutant tumors.

Ferroptosis eliminates cells damaged by oxidative stress or nutrient deprivation in the environment. It also removes malignant cells via a non-apoptotic form of cell death and plays a crucial role in suppressing tumor growth (16,30). Mounting evidence indicates that ferroptosis susceptibility shows a close association with therapeutic response. In addition, the remodeling of ferroptosis-related metabolic pathways enables tumor cells to survive under drug-induced oxidative stress (31). In the resistant models used in the present study, transcriptomic analysis revealed noticeable alterations in the ferroptosis pathway. Subsequent molecular validation demonstrated the increased expression of ferroptosis-suppressive molecules such as GPX4 and GCLM, together with reduced intracellular ROS levels. These findings suggest that acquired KRAS G12C inhibition resistance is accompanied by the reinforcement of cellular antioxidant capacity rather than merely the reactivation of canonical oncogenic signaling pathways. This concept also aligns with previous evidence demonstrating that alterations in ferroptosis sensitivity can exert an influence on the response of KRAS G12C-mutant tumors to targeted therapy (21).

The SLC7A11-GSH-GPX4 axis is considered the primary cellular defense against ferroptosis. As the functional light-chain component of system Xc-, SLC7A11 mediates the uptake of cystine in exchange for intracellular glutamate (32). Then, the imported cystine is reduced to cysteine and utilized for GSH synthesis (33). Glutamate-cysteine ligase comprises catalytic and modifier subunits GCLC and GCLM, respectively (34). It catalyzes the rate-limiting step of GSH synthesis. GPX4 uses GSH for reducing phospholipid hydroperoxides and thereby suppressing lipid peroxidation (32,35). For this reason, the coordinated upregulation of GPX4 and GCLM may provide resistant cells with a strengthened capacity to buffer oxidative stress. In this context, the decreased ROS levels noticed in resistant cells may reflect the enhanced antioxidant capacity related to acquired resistance. Thanks to this reinforced antioxidant defense, resistant cells may be able to limit oxidative damage and maintain survival.

A critical finding of the present study is that the expression of PRMT1 was elevated in KRAS G12Ci-resistant cells. PRMT1 as the primary type I protein arginine methyltransferase regulates a broad spectrum of biological processes through methylating histone and non-histone substrates (22). Aberrant PRMT1 activity exhibits an association with tumor proliferation, metabolic remodeling, transcriptional regulation and therapeutic resistance. For instance, PRMT1 has been perceived to alter chromatin accessibility and contribute to chemotherapy resistance in pancreatic cancer (36). It also activates epidermal growth factor receptor-related signaling through the H4R3me2a-dependent recruitment of SWI/SNF-related, matrix-associated, actin-dependent regulator of chromatin, subfamily a, member 4 in colorectal cancer (37), and modulates antitumor immunity in melanoma (38). These findings indicate that the biological consequences of PRMT1 activity may vary across different tumor contexts.

PRMT1 catalyzes the asymmetric dimethylation of H4R3me2a, which is a chromatin modification generally associated with transcriptional activation (39,40). Importantly, prior research has demonstrated the enrichment of PRMT1 and H4R3me2a at the SLC7A11 promoter and the enhancement of SLC7A11 promoter activity by PRMT1 (27). In the present study, ChIP-qPCR further showed that pharmacologically inhibiting PRMT1 significantly reduced the enrichment of H4R3me2a at the SLC7A11 promoter. Together, these findings

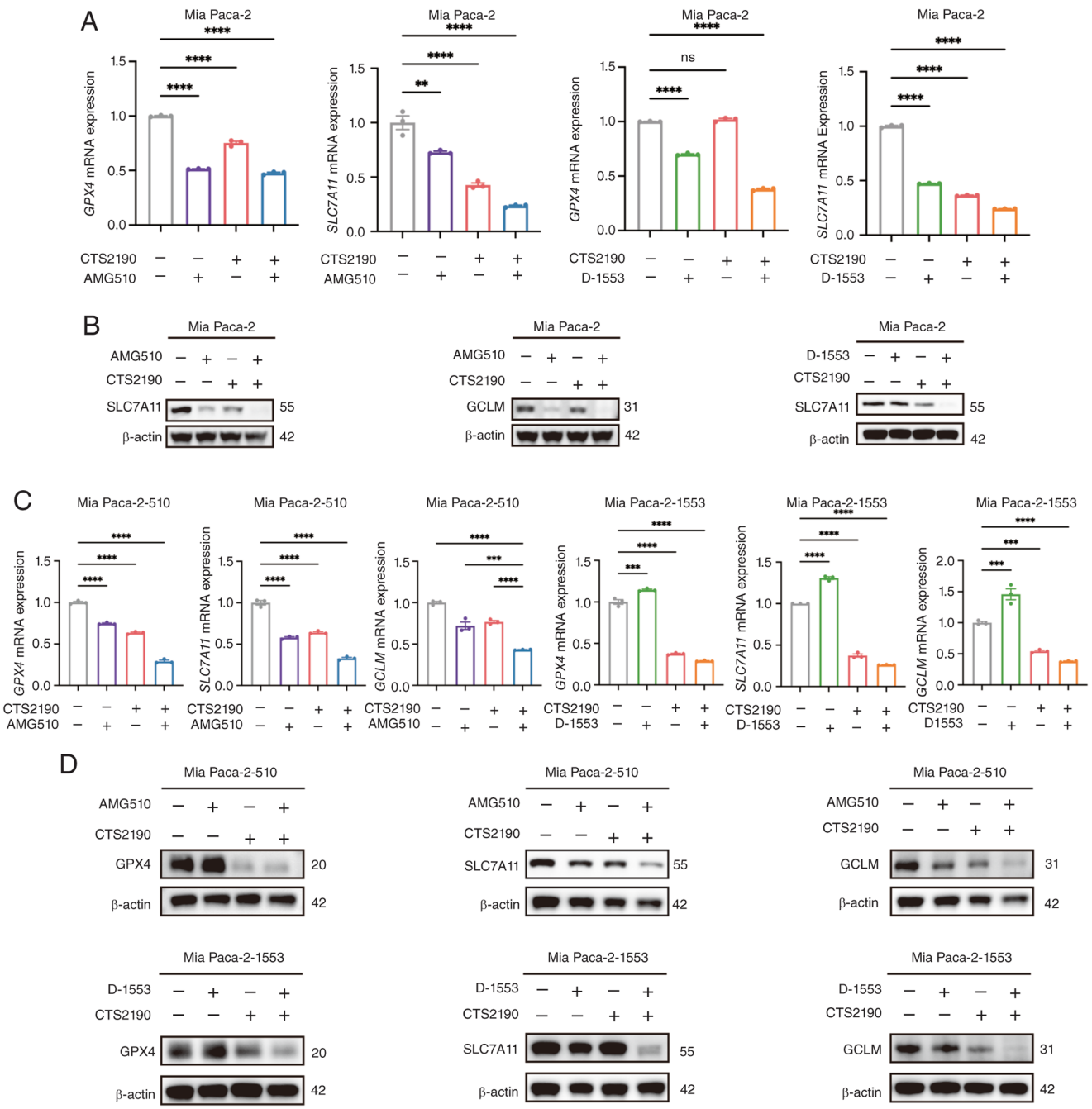


Figure 8. Combined inhibition of KRAS G12C and protein arginine methyltransferase 1 suppresses the SLC7A11-GSH-GPX4 ferroptosis defense axis in parental and resistant cells. (A) RT-qPCR analysis of *GPX4* and *SLC7A11* mRNA expression in Mia Paca-2 cells following treatment with AMG510 or D-1553, CTS2190, or the indicated combinations (n=3). (B) Western blot analysis of SLC7A11 and GCLM protein expression in Mia Paca-2 cells following the indicated treatments. (C) RT-qPCR analysis of *GPX4*, *SLC7A11*, and *GCLM* mRNA expression in Mia Paca-2-510 and Mia Paca-2-1553 cells following treatment with the corresponding KRAS G12C inhibitor, CTS2190, or their combination (n=3). (D) Western blot analysis of GPX4, SLC7A11 and GCLM protein expression in Mia Paca-2-510 and Mia Paca-2-1553 cells following the indicated treatments. Data are presented as the mean ± SEM. One-way ANOVA for multi-group comparisons. **P<0.01, ***P<0.001 and ****P<0.0001. RT-qPCR, reverse transcription-quantitative PCR; GPX4, glutathione peroxidase 4; SLC7A11, solute carrier family 7 member 11; ns, not statistically significant.

are consistent with the involvement of a PRMT1-associated H4R3me2a-SLC7A11-GSH-GPX4 axis in the present experimental system. However, this pathway should not be considered the exclusive mechanism underlying the observed phenotype. PRMT1 has been reported to regulate ferroptosis through distinct pathways in different biological contexts, including ACSL1-, FSP1-, and EGR1/GLS2-dependent mechanisms (23-26). These context-dependent effects may reflect differences in cellular lineage, oncogenic background, metabolic state and downstream PRMT1-regulated programs. As these alternative pathways were not examined in the present study, their contributions cannot be excluded and require further investigation.

These findings suggest that PRMT1-associated signaling may represent a potential therapeutic target in KRAS G12Ci-resistant tumors. The combined inhibition of KRAS

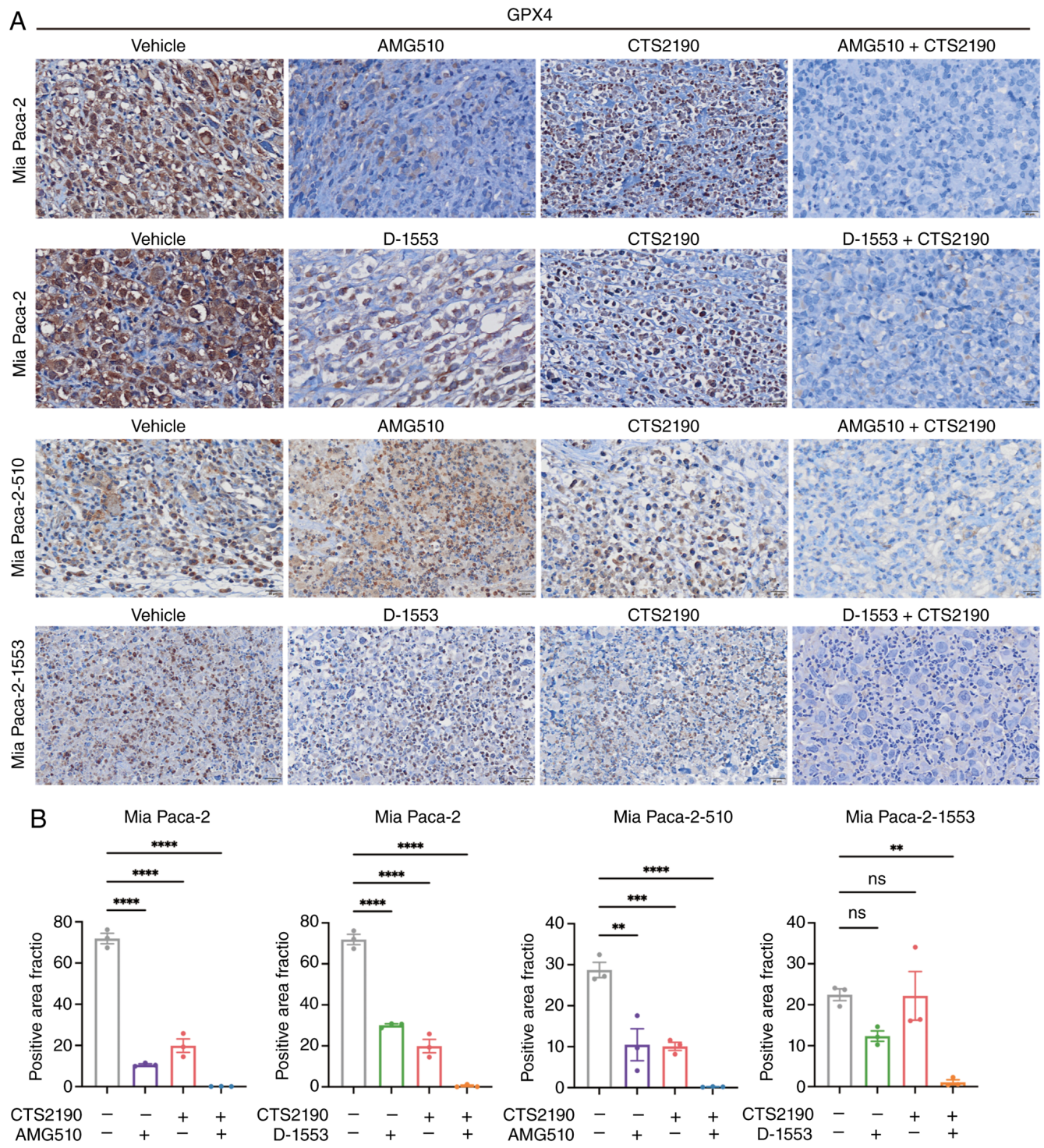


Figure 9. Combined inhibition of KRAS G12C and protein arginine methyltransferase 1 reduces GPX4 expression in parental and resistant xenograft tumors. (A) Representative immunohistochemical staining of GPX4 in Mia Paca-2, Mia Paca-2-510 and Mia Paca-2-1553 xenograft tumors following treatment with vehicle, the corresponding KRAS G12C inhibitor, CTS2190, or their combination. Scale bars, 20 μm. (B) Quantification of the GPX4-positive area fraction in the corresponding tumor tissues (n=3). Data are presented as the mean ± SEM. One-way ANOVA for multi-group comparisons. **P<0.01, ***P<0.001 and ****P<0.0001. GPX4, glutathione peroxidase 4; ns, not statistically significant.

G12C and PRMT1 produced greater antitumor activity than either treatment alone and retained efficacy in resistant models, which supported PRMT1 targeting as a strategy for mitigating acquired resistance. Of note, however, the magnitude of antitumor response was more modest in resistant xenograft models than in the parental Mia Paca-2 model. In particular, CTS2190 monotherapy demonstrated limited activity in the Mia Paca-2-1553 xenograft model, while the combination treatment still significantly suppressed tumor growth. This pattern suggests that PRMT1 inhibition alone is insufficient to fully inhibit established resistant tumors but is able to enhance their response to KRAS G12C inhibition. Thus, it appears that the combination partially resensitizes resistant tumors instead of completely restoring the response observed in

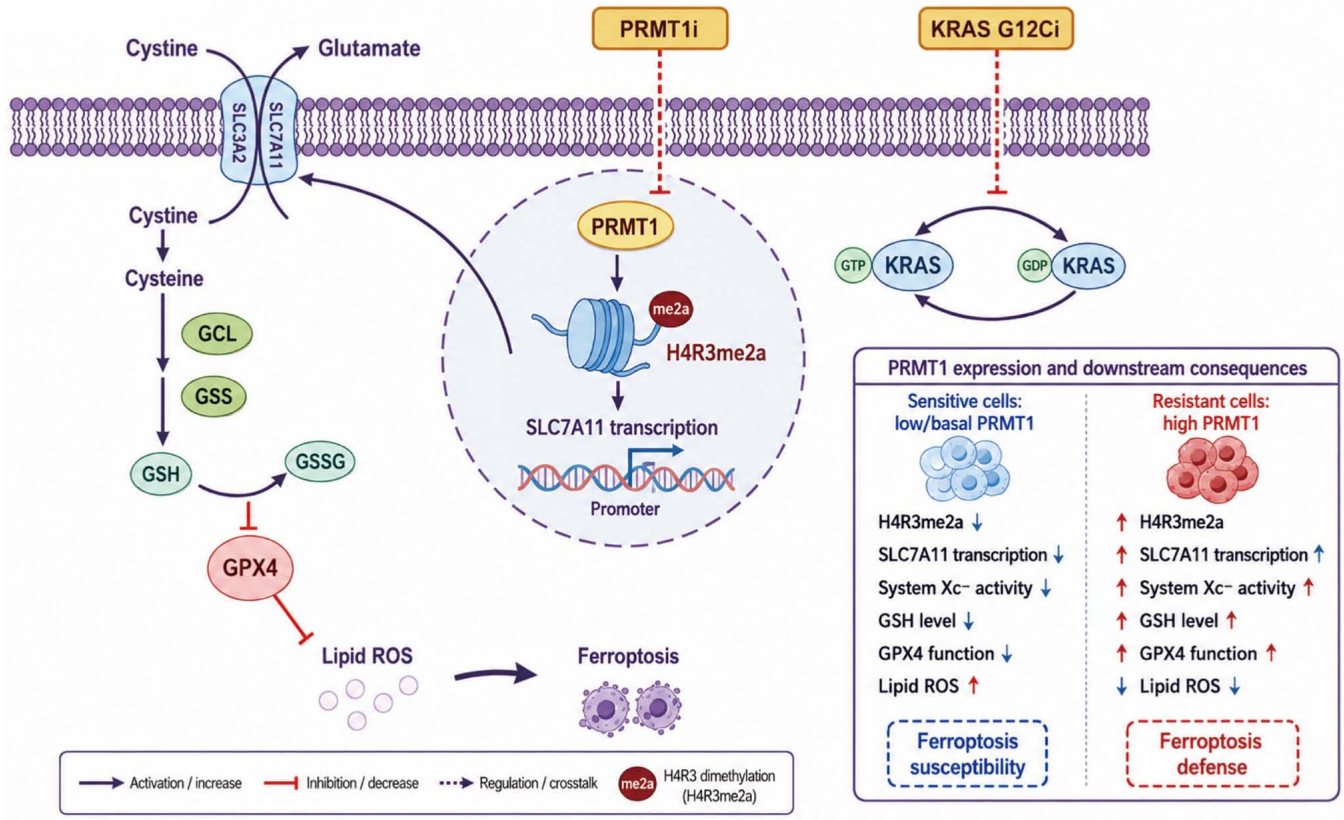


Figure 10. Schematic model of ferroptosis induction by combined KRAS G12Ci and PRMT1i. Combined treatment with KRAS G12Ci and PRMT1i suppresses the SLC7A11-GSH-GPX4 axis, leading to increased lipid peroxidation and ultimately promoting ferroptosis. PRMT1, protein arginine methyltransferase 1; PRMT1i, PRMT1 inhibition; GPX4, glutathione peroxidase 4; ROS, reactive oxygen species; SLC7A11, solute carrier family 7 member 11.

parental tumors. This partial resensitization was accompanied by increased ferroptosis susceptibility, supporting a contribution of ferroptosis to the antitumor effects of the combination treatment.

However, several limitations should be considered. First, only one KRAS G12C-mutant cell line was examined for each tumor type, which may limit the generalizability of the findings. Second, the lack of genetic validation and the potential activity of CTS2190 toward other type I PRMTs limit definitive attribution of the observed effects specifically to PRMT1. Alternative PRMT1-dependent ferroptosis mechanisms, including ACSL1-, FSP1- and EGR1/GLS2-related pathways, were not directly examined. Third, the stability of β-actin and GAPDH across parental and resistant cells was not independently validated, which may affect the quantitative interpretation of the western blot data. Fourth, the use of severely immunodeficient NCG mice precluded evaluation of the tumor immune microenvironment. Finally, the temporal role and clinical relevance of PRMT1 upregulation during resistance acquisition require further validation in longitudinal studies and patient-derived models.

From a translational perspective, PRMT1-associated signaling may represent a therapeutic vulnerability in KRAS G12C-resistant tumors. CTS2190, an orally bioavailable PRMT1-targeting/type I PRMT inhibitor, has entered early-phase clinical evaluation in advanced solid tumor patients. Available clinical data suggest that CTS2190 has a manageable safety profile. However, hematologic toxicity, especially thrombocytopenia, has been found and should be considered during further development (41). CTS2190 has been developed with preferential activity toward PRMT1. Nevertheless, its activity within the broader type I PRMT family should also be taken into consideration when target specificity is interpreted (42). Moreover, systemic PRMT1 inhibition may affect normal tissues because PRMT1 participates broadly in transcriptional regulation, DNA damage repair and other physiological processes. In the present study, serum transaminase levels indicated no apparent hepatotoxicity, but this assessment failed to exclude hematologic or other organ toxicities. Therefore, it is necessary to comprehensively evaluate systemic toxicity, pharmacokinetics, therapeutic window and tolerability before CTS2190 can be further developed in combination with KRAS G12Ci. Future studies should also determine whether PRMT1 expression, H4R3me2a status or ferroptosis-associated biomarkers have a relationship with clinical resistance and could be beneficial to identifying patients most likely to benefit from this combination strategy. The translational potential of this therapeutic approach will be further clarified by validation in patient-derived specimens, organoids and clinically derived resistant models.

Acknowledgements

Not applicable.

Funding

The present study was supported by the National Natural Science Foundation of China (grant nos. 82271876 and 82606273), the Strategic Priority Research Program of the Chinese Academy of Sciences (grant no. XDB1020000), the 'Jian Bing Ling Yan + X' R&D Program of Zhejiang (grant nos. 2025SDXT002-2 and 2026C02A1108) and the Zhejiang Medical and Health Science and Technology Plan Project (grant no. WKJ-ZJ-2418).

Availability of data and materials

The data generated in the present study may be found in the NCBI Gene Expression Omnibus database under accession number GSE346726 or at the following URL: https://www.ncbi.nlm.nih.gov/geo/query/acc.cgi?acc=GSE346726.

Authors' contributions

XF conceptualized the study, provided resources, conducted formal analysis and investigation, wrote the original draft, and wrote, reviewed and edited the manuscript. ZW conducted formal analysis and investigation, wrote the original draft, and wrote, reviewed and edited the manuscript. XY curated data, performed software and formal analysis, conducted investigation, and wrote, reviewed and edited the manuscript. HSo wrote the original draft, and wrote, reviewed and edited the manuscript. HSi, YF, YL and LX conceptualized the study, conducted investigation, and wrote, reviewed and edited the manuscript. KZ conducted investigation, and wrote, reviewed and edited the manuscript. YW conceptualized the study, curated data, conducted formal analysis and investigation, and wrote, reviewed and edited the manuscript. RG and RM conducted investigation, and wrote, reviewed and edited the manuscript. ZS provided resources, conducted investigation, and wrote, reviewed and edited the manuscript. XF and ZW confirm the authenticity of all the raw data. All authors read and approved the final version of the manuscript.

Ethics approval and consent to participate

The animal experiments involved in the present study were approved by Hangzhou Institute of Medicine Animal Experiment Ethics Committee (approval no. AP2024-07-0009; Hangzhou, China).

Patient consent for publication

Not applicable.

Competing interests

The authors disclose a patent application related to this work (application no. 2025116798151; publication no. CN121695285A; assignee: Zhejiang Cancer Hospital; inventors: Zhengbo Song, Ling Xie, Xiaoshuang Fu, Yuce Wei, Han Si, Haolin Song and Yuchen Fei; jurisdiction: CN; title: A pharmaceutical combination for treating KRAS-mutant tumors, and its preparation method and application; publication date: March 20, 2026). The authors declare no other competing interests.

References

1. Awad MM, Liu S, Rybkin II, Arbour KC, Dilly J, Zhu VW, Johnson ML, Heist RS, Patil T, Riely GJ, *et al*: Acquired resistance to KRAS(G12C) inhibition in cancer. N Engl J Med 384: 2382-2393, 2021.
2. Prior IA, Lewis PD and Mattos C: A comprehensive survey of Ras mutations in cancer. Cancer Res 72: 2457-2467, 2012.
3. Mohanty A, Nam A, Srivastava S, Jones J, Lomenick B, Singhal SS, Guo L, Cho H, Li A, Behal A, *et al*: Acquired resistance to KRAS G12C small-molecule inhibitors via genetic/nongenetic mechanisms in lung cancer. Sci Adv 9: eade3816, 2023.
4. Christensen JG, Olson P, Briere T, Wiel C and Bergo MO: Targeting Kras(g12c)-mutant cancer with a mutation-specific inhibitor. J Intern Med 288: 183-191, 2020.
5. Ryan MB, Fece de la Cruz F, Phat S, Myers DT, Wong E, Shahzade HA, Hong CB and Corcoran RB: Vertical pathway inhibition overcomes adaptive feedback resistance to $KRAS^{G12C}$ inhibition. Clin Cancer Res 26: 1633-1643, 2020.
6. Koga T, Suda K, Fujino T, Ohara S, Hamada A, Nishino M, Chiba M, Shimoji M, Takemoto T, Arita T, *et al*: KRAS secondary mutations that confer acquired resistance to KRAS G12C inhibitors, sotorasib and adagrasib, and overcoming strategies: Insights from in vitro experiments. J Thorac Oncol 16: 1321-1332, 2021.
7. No authors listed: FDA approves first KRAS inhibitor: Sotorasib. Cancer Discov 11: Of4, 2021.
8. Klomp JE, Lee YS, Goodwin CM, Papke B, Klomp JA, Waters AM, Stalnecker CA, DeLiberty JM, Drizyte-Miller K, Yang R, *et al*: CHK1 protects oncogenic KRAS-expressing cells from DNA damage and is a target for pancreatic cancer treatment. Cell Rep 37: 110060, 2021.
9. Wood K, Hensing T, Malik R and Salgia R: Prognostic and predictive value in KRAS in non-small-cell lung cancer: A review. JAMA Oncol 2: 805-812, 2016.
10. Keane F, Chou JF, Walch H, Schoenfeld J, Singhal A, Cowzer D, Harrold E, O'Connor CA, Park W, Varghese A, *et al*: Precision medicine for pancreatic cancer: Characterizing the clinicogenomic landscape and outcomes of KRAS G12C-mutated disease. J Natl Cancer Inst 116: 1429-1438, 2024.
11. Liu C, Zheng S, Wang Z, Wang S, Wang X, Yang L, Xu H, Cao Z, Feng X, Xue Q, *et al*: KRAS-G12D mutation drives immune suppression and the primary resistance of anti-PD-1/PD-L1 immunotherapy in non-small cell lung cancer. Cancer Commun (Lond) 42: 828-847, 2022.
12. Mugarza E, van Maldegem F, Boumelha J, Moore C, Rana S, Llorian Sopena M, East P, Ambler R, Anastasiou P, Romero-Clavijo P, *et al*: Therapeutic KRA^{SG12C} inhibition drives effective interferon-mediated antitumor immunity in immunogenic lung cancers. Sci Adv 8: eabm8780, 2022.
13. Ou SI, Jänne PA, Leal TA, Rybkin II, Sabari JK, Barve MA, Bazhenova L, Johnson ML, Velastegui KL, Cilliers C, *et al*: First-in-human Phase I/IB dose-finding study of adagrasib (MRTX849) in patients with advanced KRA^{SG12C} solid tumors (KRYSTAL-1). J Clin Oncol 40: 2530-2538, 2022.
14. Rohatgi A and Govindan R: Targeting KRAS G12C mutation in lung adenocarcinoma. Lung Cancer 165: 28-33, 2022.
15. Lito P, Solomon M, Li LS, Hansen R and Rosen N: Allele-specific inhibitors inactivate mutant KRAS G12C by a trapping mechanism. Science 351: 604-608, 2016.
16. Tang D, Chen X, Kang R and Kroemer G: Ferroptosis: Molecular mechanisms and health implications. Cell Res 31: 107-125, 2021.
17. Jiang X, Stockwell BR and Conrad M: Ferroptosis: Mechanisms, biology and role in disease. Nat Rev Mol Cell Biol 22: 266-282, 2021.
18. Zheng J and Conrad M: The metabolic underpinnings of ferroptosis. Cell Metab 32: 920-937, 2020.
19. Hong T, Lei G, Chen X, Li H, Zhang X, Wu N, Zhao Y, Zhang Y and Wang J: PARP inhibition promotes ferroptosis via repressing SLC7A11 and synergizes with ferroptosis inducers in BRCA-proficient ovarian cancer. Redox Biol 42: 101928, 2021.
20. Chen P, Li X, Zhang R, Liu S, Xiang Y, Zhang M, Chen X, Pan T, Yan L, Feng J, *et al*: Combinative treatment of β-elemene and cetuximab is sensitive to KRAS mutant colorectal cancer cells by inducing ferroptosis and inhibiting epithelial-mesenchymal transformation. Theranostics 10: 5107-5119, 2020.

21. Wang K, Zhang X, Fan Y, Zhou L, Duan Y, Li S, Sun Z, Zhang C, Yang H, Yuan W, *et al*: Reactivation of MAPK-SOX2 pathway confers ferroptosis sensitivity in $KRAS^{G12C}$ inhibitor resistant tumors. Redox Biol 78: 103419, 2024.
22. Shen S, Zhou H, Xiao Z, Zhan S, Tuo Y, Chen D, Pang X, Wang Y and Wang J: PRMT1 in human neoplasm: Cancer biology and potential therapeutic target. Cell Commun Signal 22: 102, 2024.
23. Zhou L, Jia X, Shang Y, Sun Y, Liu Z, Liu J, Jiang W, Deng S, Yao Q, Chen J and Li H: PRMT1 inhibition promotes ferroptosis sensitivity via ACSL1 upregulation in acute myeloid leukemia. Mol Carcinog 62: 1119-1135, 2023.
24. Li H, Qi X, He L, Yang H and Ju H: PRMT1 promotes radiotherapy resistance in glioma stem cells by inhibiting ferroptosis. Jpn J Radiol 43: 129-137, 2025.
25. Zhang X, Duan Y, Li S, Zhang Z, Peng L, Ma X, Wang T, Xiang S, Chen G, Zhou D, *et al*: CRISPR screening identifies PRMT1 as a key pro-ferroptotic gene via a two-layer regulatory mechanism. Cell Rep 43: 114662, 2024.
26. Li M, Hu L, Ke Q, Li Z, Ruan C, Lu H and Liu X: Arginine methyltransferase PRMT1 promotes ferroptosis through EGR1/GLS2 axis in sepsis-related acute lung injury. Commun Biol 8: 159, 2025.
27. Cao N, Zhang F, Yin J, Zhang J, Bian X, Zheng G, Li N, Lin Y and Luo L: LPCAT2 inhibits colorectal cancer progression via the PRMT1/SLC7A11 axis. Oncogene 43: 1714-1725, 2024.
28. Livak KJ and Schmittgen TD: Analysis of relative gene expression data using real-time quantitative PCR and the 2(-Delta Delta C(T)) method. Methods 25: 402-408, 2001.
29. Vitiello PP, Valsecchi AA, Duregon E, Di Celle PF, Cassoni P, Papotti M, Bardelli A, and Di Maio M: KRAS G12C inhibition in solid tumors: Biological breakthroughs, clinical evidence, and open challenges. Cancers (Basel) 17: 2803, 2025.
30. Fearnhead HO, Vandenabeele P and Vanden Berghe T: How do we fit ferroptosis in the family of regulated cell death? Cell Death Differ 24: 1991-1998, 2017.
31. Lei G, Zhuang L and Gan B: Targeting ferroptosis as a vulnerability in cancer. Nat Rev Cancer 22: 381-396, 2022.
32. Koppula P, Zhang Y, Zhuang L and Gan B: Amino acid transporter SLC7A11/xCT at the crossroads of regulating redox homeostasis and nutrient dependency of cancer. Cancer Commun (Lond) 38: 12, 2018.
33. Liu X, Olszewski K, Zhang Y, Lim EW, Shi J, Zhang X, Zhang J, Lee H, Koppula P, Lei G, *et al*: Cystine transporter regulation of pentose phosphate pathway dependency and disulfide stress exposes a targetable metabolic vulnerability in cancer. Nat Cell Biol 22: 476-486, 2020.
34. Chen Y, Yan Q, Ruan S, Cui J, Li Z, Zhang Z, Yang J, Fang J, Liu S, Huang S, *et al*: GCLM lactylation mediated by ACAT2 promotes ferroptosis resistance in $KRAS^{G12D}$-mutant cancer. Cell Rep 44: 115774, 2025.
35. Lu SC: Regulation of glutathione synthesis. Mol Aspects Med 30: 42-59, 2009.
36. Ku B, Eisenbarth D, Baek S, Jeong TK, Kang JG, Hwang D, Noh MG, Choi C, Choi S, Seol T, *et al*: PRMT1 promotes pancreatic cancer development and resistance to chemotherapy. Cell Rep Med 5: 101461, 2024.
37. Yao B, Gui T, Zeng X, Deng Y, Wang Z, Wang Y, Yang D, Li Q, Xu P, Hu R, *et al*: PRMT1-mediated H4R3me2a recruits SMARCA4 to promote colorectal cancer progression by enhancing EGFR signaling. Genome Med 13: 58, 2021.
38. Tao H, Jin C, Zhou L, Deng Z, Li X, Dang W, Fan S, Li B, Ye F, Lu J, *et al*: PRMT1 inhibition activates the interferon pathway to potentiate antitumor immunity and enhance checkpoint blockade efficacy in melanoma. Cancer Res 84: 419-433, 2024.
39. Zhang X and Cheng X: Structure of the predominant protein arginine methyltransferase PRMT1 and analysis of its binding to substrate peptides. Structure 11: 509-520, 2003.
40. Yang Y and Bedford MT: Protein arginine methyltransferases and cancer. Nat Rev Cancer 13: 37-50, 2013.
41. Jin J, Yao J, Li W, Wang M, Zhou H, Wang Q, Yang J, Li Z, Xing S, Wu H, *et al*: Efficacy and safety results of a first-in-class PRMT1 inhibitor CTS2190 in patients (pts) with immune checkpoint inhibitor (ICI)-insensitive advanced solid tumors. J Clin Oncol 44 (Suppl 16): e15164, 2026.
42. Shi H, Fu X, Ouyang Q, Huang J, Wang Y, Wang Y, Xu G, Mi Y and Wu H: Abstract 6279: CTS2190, a next-generation epigenetic inhibitor for targeting type I PRMT deregulated human tumors. Cancer Res 83 (Suppl 7): S6279, 2023.
43. Jiang S, Li H, Zhang L, Mu W, Zhang Y, Chen T, Wu J, Tang H, Zheng S, Liu Y, *et al*: Generic diagramming platform (GDP): A comprehensive database of high-quality biomedical graphics. Nucleic Acids Res 53: D1670-D1676, 2025.



Copyright © 2026 Fu et al. This work is licensed under a Creative Commons Attribution-NonCommercial 4.0 International (CC BY-NC 4.0) License.